

[entry]nyt/global/

UNIVERSITÉ DE GENÈVE

EMBL

Section de chimie et biochimie Cell Biology and Biophysics
Unit

Department de biochimie

Dr. Jonas Ries

Professeur Marko Kaksonen

REGULATION OF MEMBRANE SCISSION IN YEAST ENDOCYTOSIS

THÈSE

présentée à la Faculté des sciences de l'Université de Genève
pour obtenir le grade de Docteur ès sciences, mention
biochimie

par

Deepikaa Menon

de

Chennai (India)

Thèse N° xxxx

GENÈVE / HEIDELBERG
photoshop EMBL
2018

Abstract

Some other stuff that happened

Clathrin-mediated endocytosis is an essential cellular process to take up cargo molecules from the cell surface. More than 50 proteins form the underlying macromolecular machinery, which is highly conserved among eukaryotes. Understanding its structural organization is key to unraveling the architectural principles that allow the endocytic machinery to form vesicles with high efficiency and regularity. However due to its small size, complexity and fast dynamics, it is still mostly unknown how endocytic proteins are arranged *in situ*.

I have used single-molecule localization based superresolution microscopy to image endocytic sites in fixed budding yeast *Saccharomyces cerevisiae* with high spatial resolution, and found an intricate structural organization of proteins within the endocytic machinery.

Using high-throughput localization microscopy, I imaged tens of thousands of endocytic sites and revealed a striking radial organization of endocytic proteins, where each endocytic functional module occupies a distinct radial zone. Over the endocytic time line, protein assemblies increase in size as well as in regularity. The initial phase of endocytosis is characterized by variable structures, while in the late phase proteins assemble with a higher degree of radial order. I discovered that actin polymerization, which is essential for endocytosis in yeast, is spatially predetermined by nucleation promoting factors to occur exclusively around the coat, and that proteins, which couple actin to the plasma membrane, are located at the center of the coat. This circular pre-patterning provides an elegant explanation for how the actin machinery is able to efficiently generate and transfer force to invaginate the plasma membrane. In the outermost radial zone, an endocytic myosin possibly pulls actin filaments outwards to facilitate membrane invagination.

I established a novel approach to reconstruct temporal information of fixed endocytic sites by integrating the images with centroid trajectories from living cells, and obtained a time-resolved superresolution visualization of the highly dynamic mobile phase of endocytosis. This shows

that the actin network emerges from a nucleation zone at the base of the plasma membrane, which is determined by nucleation promoting factors.

I therefore propose that the endocytic machinery undergoes a structural transition after an initial phase with variable timing and structures, toward the regular late phase, in which endocytic proteins are radially organized around the coat. A robustly pre-patterned actin nucleation zone prepares the endocytic machinery for the onset of actin polymerization, which represents a key mechanistic step and marks the transition point into the mobile phase, where the coat is rapidly internalized and a vesicle is formed.

Zusammenfassung

Clathrin-vermittelte Endozytose ist ein essenzieller zellulärer Prozess, um Moleküle von der Zelloberfläche aufzunehmen. Mehr als 50 Proteine bilden die zugrundeliegende makromolekulare Maschinerie, welche in Eukaryoten höchst konserviert ist. Um ihre Konstruktionsweise zu verstehen, welche eine Vesikelbildung mit hoher Effizienz und Regelmäßigkeit erlaubt, ist es notwendig zu untersuchen, wie endozytotische Proteine strukturell organisiert sind. Aufgrund der kleinen Größe, Komplexität und Dynamik der endozytotischen Maschinerie ist die Anordnung dieser Proteine *in situ* jedoch größtenteils unbekannt.

Ich habe Einzelmolekül-Lokalisationsmikroskope verwendet, um endozytotische Strukturen in fixierten Zellen von Bäckerhefe *Saccharomyces cerevisiae* mit hoher räumlicher Auflösung abzubilden. Dabei habe ich eine komplexe Organisation der endozytotischen Proteinen festgestellt.

Mithilfe von Hochdurchsatz-Lokalisationsmikroskopie konnte ich zehntausende endozytotische Strukturen untersuchen. Dabei habe ich eine bemerkenswerte radiale Ordnung gefunden, in welcher die funktionalen Module festgelegte radiale Bereiche besetzen. Je weiter Endozytose fortgeschreitet, desto größer und regelmäßiger werden die Strukturen. Zu Beginn sind die Anordnungen vielfältig in Größe und Form, während sie später einen hohen radialen Organisationsgrad aufweisen. Ich habe entdeckt, dass Aktin-Polymerisation, welche in Hefe zur Endozytose benötigt wird, nur in einem durch Aktin-Nukleirungsfaktoren bestimmten, ringförmigen Bereich auftritt. Dieser Bereich bildet sich um eine Proteinschicht herum, in welcher Proteine die Plasmamembran mit dem Aktinnetzwerk verknüpfen. Durch dieses Ringmuster kann die notwendige Kraft, um die Plasmamembrane einzustülpen, durch die Bildung eines Aktinnetzwerkes effizient erzeugt und auf die Membran übertragen werden. In einem äußeren Ring zieht ein endozytotischer Myosin-Motor möglicherweise das Aktin-Netzwerk auseinander, um den Einstülpungsprozess zu unterstützen.

Ich habe ein neues Konzept entwickelt, um den endozytotischen Zeitpunkt von fixierten Strukturen direkt aus den hochaufgelösten Bildern

zu bestimmen, indem sie mithilfe von Fluoreszenz-Partikelverfolgungs-Daten aus lebenden Zellen ausgewertet werden. Dadurch konnte ich die höchst dynamische mobile Phase der Endozytose mit zeitlicher und hoher räumlicher Auflösung darstellen. Diese Visualisierung zeigte direkt, dass sich das Aktin-Netzwerk aus einer Nukleierungszone auf der Plasmamembran bildet, welche durch Nukleirungsfaktoren gebildet wird.

Ich schlage deshalb ein Modell vor, wie sich die endozytotische Maschinerie organisiert. Nach einer Initiierungsphase mit variablem Zeitablauf und vielfältigen Strukturen gibt es einen Übergang hin zu regelmäßigen, radial organisierten Proteinanordnungen, welche sich um die zentrale Proteinschicht bilden. Durch diese Organisation wird ein Bereich robust vorbestimmt, in welchen sich später das Aktin-Netzwerk bilden kann. Der Beginn der Aktin-Polymerisierung ist ein wichtiger mechanistischer Schritt, der den Übergang hin zur mobilen Phase der Endozytose bewirkt, in welchem schließlich das Clathrin-umhüllte Vesikel gebildet wird.

Acknowledgements

Thank you Marko, for your patience and guidance while I discovered biology, whether or not you realized what you were getting into. I feel (gratuitously) lucky to have been supervised by someone with whom I share a philosophy of science. Many thanks to the lab: Ori, Camilla, Hetty, Tanja, and Andrea, for getting me started on the messy details, your invaluable feedback throughout, and for making coming to work fun. The Geneva crew, Daniel, Mateusz, Serena, and Anne-Sophie, thanks for the many animated discussions, and for sharing weird work hours!

Thanks to Jonas and the rest of the Ries lab for shelter during the transition to Geneva. Jonas, I'm still a bit skeptical about whether it's actually healthy to eat that fast, but I will keep trying. Joran, Markus, Kostek, Jan, thank you for making limbo bearable. Markus, for the many conversations, meals, and for annoying me into becoming a better scientist. I am delighted to be the other grumpy person.

Noticeably complacent about expressing my feelings, I will take the opportunity to thank the people I am deeply indebted to for getting me through these years. Thibaut, Martina and Paul, I have been rescued many times only by your existence, thank you for existing. Anastasia, for sharing your home and friendship. Many others in Heidelberg and Geneva who have made this time enjoyable: Filipa, Marvin, Phillippe, Ori, Daniel, thank you for the company.

Last and quite far from least, the fact that this thesis exists is owed to Helke Hildebrand, Dean of the Graduate program at EMBL when I started my PhD. Thank you Helke, for the endless supply of support, encouragement, and chocolate.

I am truly grateful to many people, who I was lucky to get to know, work with, or just hang out with, and who made the last four years a unique experience.

First and foremost: Thank you Jonas, for inviting me to join your group when it had just become one, and for sharing this truly exciting time of starting a lab, when ideas turn into projects, and rooms that seem large become too small. I am really grateful for your guidance and support, your openness to my ideas and the freedom to pursue them, for keeping your door open at all times, for your physicist's approach to thinking about biology, and your respectful and enjoyable way of leading the lab. It was really fruitful and fun working with you over the past four years.

Thank you Marko, for being a second supervisor to me, and quasi adopting me into your lab. It was a privilege working with you and your group. Your collaborative spirit is truly inspiring and a great, productive way to do science.

I would like to thank my TAC members Michael Knop and Edward Lemke, for great scientific discussions during my committee meetings. Your external view and direct feedback was most appreciated, and really helped me during my PhD. Thank you, Michael and Marko, for reviewing this thesis, and Ulrich Schwarz for agreeing to participate in the defense.

Thank you, all you cool people who are and were in the Ries lab! Thank you Ulf, Joran, Kostek, Li-Ling, Jervis, Johannes, Raja, Tooba, Rohit, Sunil, Jan, Johannes, Manuel, Asia, Silvia, Sven and Andreas - we surely have a great working atmosphere in the lab and had amazing retreats, BBQs and lab day actions. You guys made the Ries lab an awesome place to do a PhD.

Merci Joran, you are a great friend, colleague and desk neighbor. Having you in the lab is a gift, and working with you is absolutely awesome. Thanks for all the french curses, it is such a great feeling to see that somebody else can be even more grumpy than me.

Bedankt Jan, you are really one of us! Thank you for your work, your commitment and the dutchiness you brought to the lab. Who thought someone could stay longer than Rohit.

Thank you Kaksonens for taking me in for your group meetings! Thanks Tanja and Andrea for getting me started into the yeast world, and of course also Dominik, Camilla, Hetty, Ori and Deepikaa. Thank you Ori and Deepikaa for staying around and keeping some Kaksonen at EMBL. Thanks Deepikaa for choosing the Ries lab for desk asylum, and being (much more than just) our grumpy receptionist. We will always have a desk for you. Maybe a small one. Ori, I admire your optimistic and thoughtful way of working and going through life, and wish you an awesome time in the next years, with everything that lies ahead.

I would like to express my gratitude to the EMBL media kitchen and the mechanical and electronic workshops for their great support of our work.

Thank you Alba, for giving me a quiet place to write!

Thanks to all you great people that made it fun to be in Heidelberg. Thanks Nik, Simon and Joran for our Doppelkopf nights with awesome Bock rounds, thanks EMBL predocs for a cool community and especially

Ale, Deepikaa, Joran, Nik, Simon and Ori, you made this time really memorable.

Last, and certainly not least, I want to thank my family. Vielen Dank, liebe Eltern, für eure Unterstützung! Lieber Jakob, du bist ein klasse Bruder, und mit deiner gelassenen Geraedlinigkeit wirklich ein Vorbild für mich.

Liebe Hanna, Worte werden dem nicht gerecht, was ich für dich fühle und dir verdanke, aber ich versuch's: Du bist eine bezaubernde, wundervolle Frau, und hast mit deiner Liebe großes Glück in mein Leben gebracht, für das ich dir innig und unendlich verbunden bin. Ohne dich, deine bedingungslose Unterstützung und Gutherzigkeit, und deine unbeschreibliche Empathie, wäre diese Arbeit nicht möglich gewesen.

Lieber Felix und liebe Nora, ihr seid die wunderbarsten Menschen, die ich kenne. Ihr seid das, worauf ich am stolzesten bin, und oft kann ich mein Glück mit euch gar nicht fassen. In Momenten, in denen alles richtig nervt, zaubert euer Lächeln einfach alles weg.

Contents

Abstract	iii
Zusammenfassung	v
Acknowledgements	vii
Contents	xi
1 Introduction	1
1.1 Endocytosis and cell trafficking pathways	1
1.2 Clathrin-mediated endocytosis	3
1.3 CME in mammalian and yeast cells	5
1.3.1 Clathrin is required for mammalian CME	5
1.3.2 Actin forces are required for yeast CME	6
1.3.3 CME in yeast is highly regular	6
1.3.3.1 Early initiation phase	7
1.3.3.2 Coat module	7
1.3.3.3 Actin module	8
1.3.3.4 Scission module	9
1.3.4 Membrane scission in mammalian cells	9
1.3.4.1 Scission is dependent on dynamin	9
1.3.4.2 Dynamin is an oligomeric GTPase	9
1.3.4.3 Dynamin interacts with BAR proteins to cause scission	10
1.3.4.4 Dynamin and BAR proteins interact via PRD and SH3 regions	10
1.3.5 Membrane scission in yeast	11
1.3.5.1 Yeast dynamin-like proteins	11
1.3.5.2 Yeast BAR domain proteins Rvs161/167 regulate scission timing	11
1.3.5.3 What causes scission?	12

1.4	BAR domain proteins	13
1.4.1	NBAR proteins and membrane shapes	14
1.4.2	NBAR protein in endocytosis: Amphiphysin	15
1.4.3	NBAR protein in endocytosis: Endophilin	15
1.4.4	NBAR protein in yeast endocytosis: the Rvs complex	16
2	Aims of the study	19
3	Results	21
3.1	Rvs localization in yeast endocytosis	21
3.2	Rvs deletion phenotype	23
3.3	Recruitment of Rvs and function of domains	23
3.3.1	BAR domain senses membrane curvature in-vivo .	25
3.3.2	The SH3 domain is able to localize Rvs in an actin and curvature-independent manner	26
3.3.3	Loss of the SH3 domain affects progression of endocytic sites	28
3.4	Scission mechanisms	31
3.4.1	Yeast dynamin Vps1	31
3.4.1.1	Membrane scission is not dependent on Vps1	31
3.4.2	Lipid hydrolysis and membrane scission	33
3.4.2.1	Synaptojanin-like Inp52 localizes to endocytic sites in the late scission stage	34
3.4.2.2	Loss of yeast synaptojanins does not significantly affect coat and Rvs dynamics .	36
3.4.3	Membrane scission as a result of protein friction .	38
3.4.3.1	Membrane scission does not occur at shorter tube lengths when amount of Rvs is increased	38
3.4.3.2	Scission timing occurs at a specific amount of Abp1, independent of the amount of Rvs recruited	39
3.4.4	BAR domains as membrane scaffolds	42
3.4.4.1	Localization of BAR domain alone prevents membrane scission	42
3.4.5	Membrane dynamics with reduced membrane tension	44

4 Discussion	45
4.1 Recruitment of Rvs to endocytic sites	45
4.1.1 Timing of localization and efficiency of recruitment	46
4.1.1.1 The BAR domain senses membrane curvature	46
4.1.1.2 BAR domain times recruitment of Rvs	46
4.1.1.3 SH3 domain regulates actin network	47
4.1.1.4 The SH3 domain makes Rvs localization efficient	48
4.1.1.5 The SH3 domain can assemble and disassemble Rvs molecules	48
4.1.2 Arrangement of Rvs	49
4.1.2.1 Rvs does not form a tight scaffold on yeast membrane tubes	49
4.1.2.2 A limit for how much Rvs can be recruited to the membrane	50
4.1.3 Rvs161 and Rvs167 are recruited as dimers to endocytic sites	51
4.1.3.1 Contribution of the N-amphiphatic helix and GPA region	51
4.2 What causes membrane scission?	51
4.2.1 Dynamin does not drive scission	51
4.2.2 Lipid hydrolysis is not the primary cause of membrane scission	52
4.2.3 Protein friction does not drive membrane scission .	53
4.2.4 Actin polymerization generates forces required for membrane scission	54
4.3 Function of the Rvs complex	54
4.3.1 A critical amount of Rvs is required to allow invaginations to grow	54
4.3.2 Rvs scaffolds membrane pore	54
4.4 Role of other scission-stage proteins	54
4.4.1 Inp52 is likely involved in uncoating vesicles after scission	54
4.5 Model for membrane scission	54
5 Materials and Methods	55
5.1 Materials	56
5.1.1 Yeast strains	56

5.1.2	Plasmids	60
5.1.3	Buffers	61
5.1.4	Media	61
5.1.5	Imaging	63
5.2	Methods	64
5.2.1	Fluorescent tagging yeast with PCR cassette insertion	64
5.2.2	Live-cell imaging	64
5.2.2.1	Live-cell Image analysis	65
5.2.2.2	Cytoplasmic background quantification for BAR versus WT Rvs167-GFP	66
5.2.2.3	CLEM	66

List of Figures

3.1	Centroid tracking yeast endocytic proteins	22
3.2	some stuff	24
3.3	Localization of Rvs167 and BAR with and without membrane curvature	27
3.4	Effect of the Rvs167 SH3 deletion	30
3.5	Rvs localization in vps deletion	32
3.6	Synaptojanin-like proteins in yeast	35
3.7	Synaptojanin deletion	37
3.8	Overexpression of the Rvs complex in haploid cells	39
3.9	Dynamics of endocytosis in diploid strains with gene duplicated Rvs	41
3.10	Progression of invagination with increasing BAR recruitment	43

List of Tables

List of Abbreviations

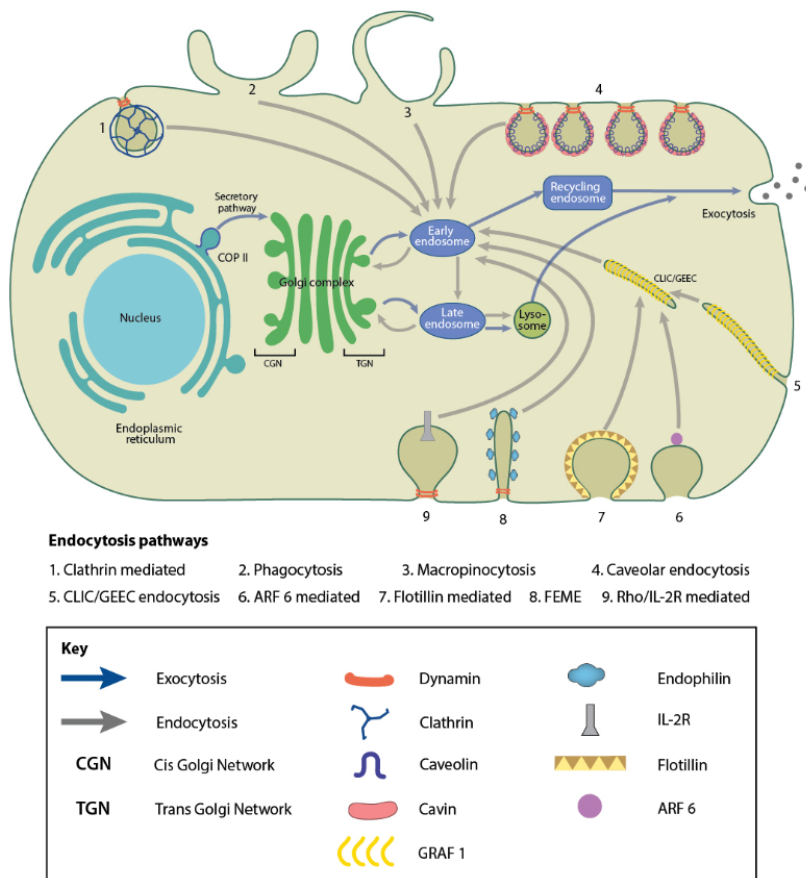
2D	Two-dimensional
3D	Three-dimensional
5-FOA	5-fluoroorotic acid
ADP	Adenosine diphosphate
ATP	Adenosine triphosphate
AF	Alexa Fluor
ANTH	AP180 N-terminal homology
CP	Capping protein
CME	Clathrin-mediated endocytosis
ConA	Concanavalin A
CLEM	Correlative light and electron microscopy
DNA	Deoxyribonucleic acid
DMSO	Dimethyl sulphoxide
EDTA	Ethylene diamine tetraacetate
EE	Early endosome
EH	Epsin homology
EM	Electron microscopy
EMCCD	Electron multiplying charge-coupled device
ENTH	Epsin N-terminal homology
ER	Endoplasmic reticulum
FRAP	Fluorescence recovery after photobleaching
LB	Lysogeny broth
MVB	Multivesicular body
NPF	Nucleation promoting factor
ORF	Open reading frame
OD₆₀₀	Optical density (600 nm)
PFA	Paraformaldehyde
PBS	Phosphate buffered saline
PIP₂	Phosphatidyl inositol (4,5) diphosphate

PEG	Poly ethylene glycol
PM	Plasma membrane
PCR	Polymerase chain reaction
RFP	Red fluorescent protein
ROI	Region of interest
RNA	Ribonucleic acid
RT	Room temperature
SH3	Src homology 3
SC	Synthetic complete
TIRF	Total internal reflection fluorescence
UIM	Ubiquitin interaction motif
UV	Ultra violet
VPS	Vacuolar protein sorting
WH	WASP homology
WASP	Wiskott-Aldrich syndrome protein
YPD	Yeast extract peptone dextrose
YPAD	Yeast extract peptone dextrose plus adenine

1 | Introduction

1.1 Endocytosis and cell trafficking pathways

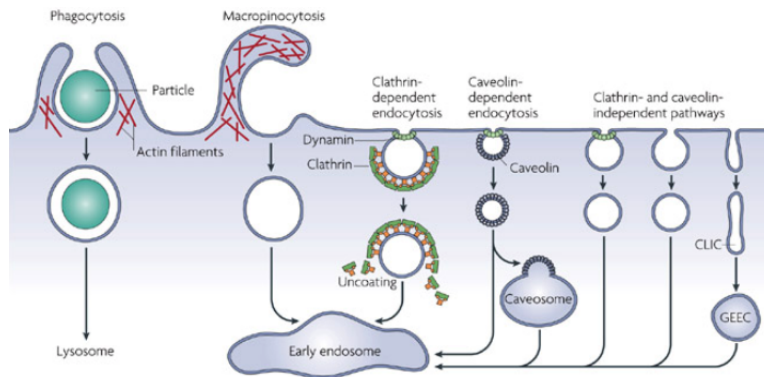
The plasma membrane serves as the defining barrier between the internal and external cell, thus creating cellular identity, and facilitating evolution out of the primordial soup into a defined structure that can regulate entry of signals into the cell. In eukaryotes, and with increasing complexity, in multicellular eukaryotes, tuning cellular response to external signals has resulted in a complex network of signaling pathways, and tight coupling of these pathways with the process of endocytosis. Endocytosis is defined as the uptake of molecules too big to pass through the plasma membrane. It involves the invagination of the plasma membrane into a cargo-filled tube, and culminates in the severing of this tube to form a cargo-filled vesicle, whose components and contents are then targeted to other cellular organelles for either degradation or recycling.



Apart from internalizing cargo, endocytosis allows regulation of the plasma membrane itself: its lipid and protein composition, and therefore many physical and biochemical properties like tension, rigidity, surface-receptor composition and localization. Cargo taken up by endocytic pathways include these surface-receptors and their ligands, that are transported across the cell, taking part in a signaling cascade, and forming the link between cell signaling and endocytosis.

Somewhat dramatically, endocytosis “constitutes the major communications infrastructure of the cell. As such, it governs almost all aspects of the relationships of the cell with the extracellular environment and of intracellular communication. Its evolution constitutes, arguably, the major driving force in the evolution of prokaryotic to eukaryotic organisms”¹. Plasma membrane regulation and internalization of signaling molecules are critical for the function of the cell. Among the vast array of important cargo that are taken up via endocytosis are cholesterol^{2,3}, insulin⁴, and other hormones. Not surprisingly, many human diseases have been linked to defects in the endocytic pathway like familial hypercholesterolemia^{2,3} -the study of which established the field of endocytosis-, Alzheimer’s⁵,

and some types of cancer⁶. The importance of the endocytic machinery as the entry portal of the cell is evident in the fact that it is hijacked by pathogens like viruses and bacteria to enter host cells⁷. Other components of the cellular signaling pathway transmit signals across the cell and between various organelles like the Golgi apparatus and endoplasmic reticulum. These membranes undergo similar transitions of the bounding membrane, and have mechanistic and biochemical similarities^{8,9}.



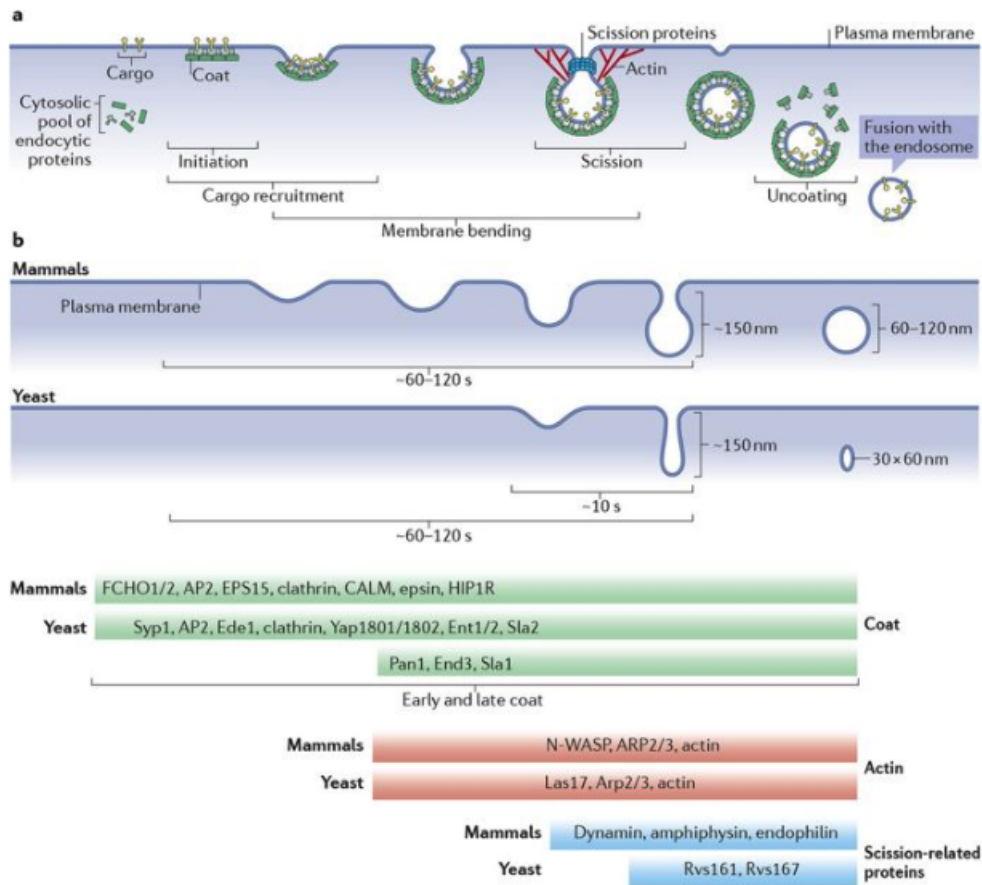
Although many early discoveries relating to endocytic pathways were identified in mammalian cell types^{10,11}, description of endocytosis in *S.cerevisiae*¹² marked the beginning of important findings that were made in the yeast and later verified in mammalian cells. The ease of genetic manipulation, availability of the completed sequence of the yeast genome, and relative simplicity of endocytic pathways- there is only one- drove several discoveries that established yeast as a powerful model organism^{13,14}.

1.2 Clathrin-mediated endocytosis

Many different endocytic pathways that facilitate the internalization of cargo at the plasma membrane exist, as depicted in Fig.2, all differing in the size and type of cargo. Of them, Clathrin-mediated endocytosis (CME), is universal among eukaryotes and contributes to 90% of cargo trafficked into the cell¹⁵. First identified by studying yolk uptake in mosquitos, ultrastructural studies of their oocytes (where the concentration of uptake events is high enough to be easily studied) identified a bristly coat formation on the cell membrane and similarly bristly vesicles, that then lost this coat and fused to eventually form yolk bodies in the mature oocyte¹⁶. The bristle was noted in several cell types, and was later identified as a lattice of a single highly conserved protein¹⁷. This protein was named

Clathrin, derived from the latin word for lattice. Clathrin is formed of light and heavy chains incorporated into a triskelion¹⁸ that assembles into closed hexagonal and pentagonal structures on the inner leaflet of the plasma membrane. Clathrin-mediated endocytosis has, since four decades ago, been recognized has an ubiquitous mechanism of membrane uptake in cell types ranging from the frog presynaptic membrane¹⁹ to rat vas deferens²⁰.

Clathrin and associated proteins do not only interact with the plasma membrane. It has also been observed localizing to the trans-golgi network (TGN); these clathrin-coated vesicles mediate traffic from the TGN to the endosome. Specification of vesicle target to different cellular compartments is achieved by Clathrin interaction with specialized adaptor proteins like the adaptor protein complexes (AP), which specify Golgi-to-early endosome traffic, while Golgi-localized gamma-adaptin (GGA) complexes specify Golgi-to-late endosome traffic. These membrane associations, among others form components of the cellular signaling pathway that transmit signals across the cell and between various organelles like the Golgi apparatus and endoplasmic reticulum. These membranes undergo similar transitions of the bounding membrane, and have some mechanistic and biochemical similarities^{13,14}.



1.3 CME in mammalian and yeast cells

1.3.1 Clathrin is required for mammalian CME

That the clathrin lattice is responsible for remodeling the plasma membrane and selecting cargo was speculated in the first papers that noted the “bristly” coat^{16,21}. In multicellular organisms like *C.elegans*, clathrin depleted by RNAi results in decreased endocytic uptake in oocytes and dead progeny²², in *D.melanogaster*, deletion of clathrin heavy chain results in embryonic lethality²³. In HeLa cells, knock-down of the heavy chain by RNAi results in decrease in endocytosis by 80%²⁴; essentially, endocytosis fails in the absence of clathrin. The exact contribution of clathrin in the progression of endocytosis has been heavily debated, but its involvement itself has not. Although several genes involved in CME in yeast were found to be homologues of the mammalian machinery, however, early work in yeast revealed that clathrin is not necessary for endocytosis²⁵. Loss of clathrin changes the size of the vesicles formed at scission, and

leads to decrease in the number of established endocytic sites^{26,27}: it appears to affect establishment of sites and regulation of scission. It became apparent that though the mammalian and yeast systems were mechanistically similar and most of the yeast endocytic proteins had mammalian homologues²⁸, there are some significant differences.

1.3.2 Actin forces are required for yeast CME

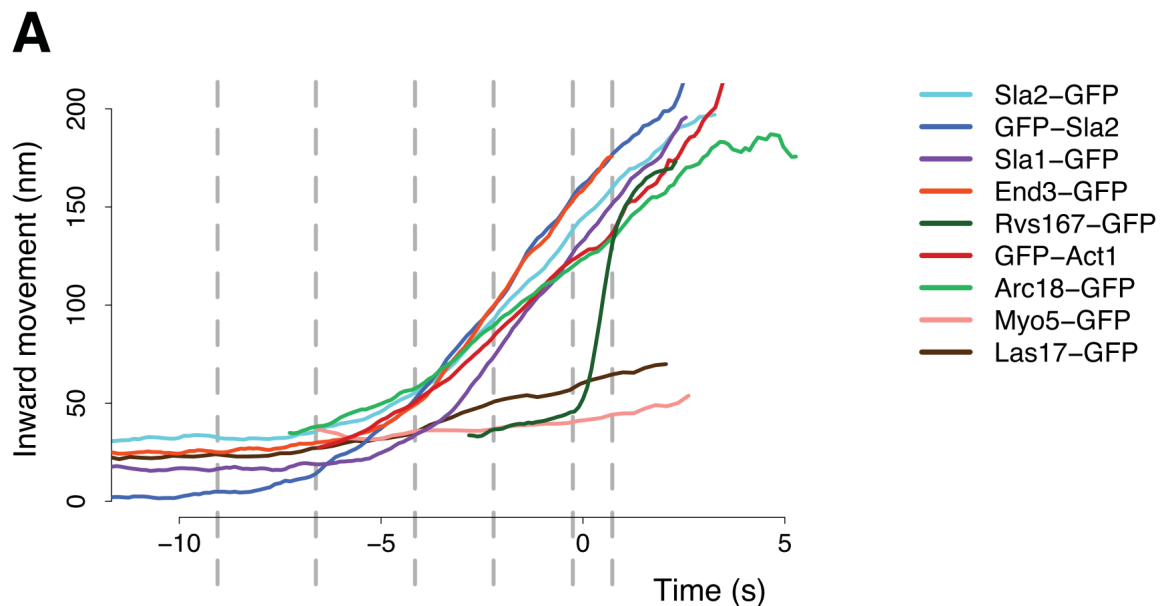
Cortical actin patches were first seen in *S.cerevisiae*, that were later established as endocytic sites from the colocalization of other endocytic proteins. While the mammalian CME uptake is heavily dependent on clathrin, the yeast system relies on actin and its proper organization for endocytosis²⁹. Not only is actin itself necessary for the initiation of plasma membrane deformation³⁰, coupling the endocytic coat to actin are necessary for internalization^{31,32}. The cell wall surrounding the plasma membrane in yeast cells induces a high intracellular turgor pressure³³, which could explain the high force requirement for membrane deformation in yeast.

1.3.3 CME in yeast is highly regular

In yeast, over fifty proteins are recruited, interact, and disassembly during this process. In mammals as well as in yeast, the proteins that arrive at an endocytic site can be distributed into different modules according to their relative time of recruitment and function. A variable initiation phase assembles coat proteins on the plasma membrane and establishes an endocytic site. While the later proteins show relatively high variability in both recruitment as well as time spent at sites in mammalian cells, in yeast this initiation is followed by a very stereotypic sequence of events that assembles coat proteins, nucleates actin, organizes the actin network, invaginates a membrane tube, and finally severs the membrane to produce cargo-filled vesicles²⁶. Coat proteins arrive upon initiation of endocytic sites, the actin and WASP modules arrive next, and includes actin nucleating proteins, actin, actin-binding proteins that organize the actin network and produce forces that begin to pull the membrane into the cytoplasm. The scission module arrives last, and regulates the final shape transitions of the endocytic site from tubular membrane to vesicle.

Stereotypicity of the post-initiation stages of yeast endocytosis has allowed averaging the behavior of various proteins from multiple endocytic events. Tracking and averaging the behavior of these proteins has led to

understanding the spatial and temporal regulation of endocytosis in remarkable detail^{26,34,35}. The multiple stages of endocytosis are discussed below.



1.3.3.1 Early initiation phase

A variable initiation phase establishes endocytic sites and selects cargo³⁶. The earliest proteins to arrive at sites, Ede1 and Syp1 are not required to form endocytic sites. Deletion of an entire seven protein set of early endocytic proteins (Ede1, Syp1, Yap1801/1802, Apl1, Pal1, Pal2) does not prevent endocytosis. It seems that the initiation of endocytosis in yeast is independent of the recruitment of any one protein, and is likely a result of several different cooperative or independent factors³⁶, that could give the process robustness in the absence of alternate pathways for uptake of essential nutrients and signals. The variability in this phase could also provide a “check-point”, to ensure that sufficient cargo is loaded²⁸ before later (energy consuming) phases are triggered.

1.3.3.2 Coat module

Coat proteins serve to template later proteins³⁵, as well as form the link between the actin module³², ingressing membrane, and cargo associated with it. Unlike in mammalian cells, as mentioned earlier, clathrin adaptors and the clathrin triskelion are not necessary for the progression of sites, although deletion of clathrin introduces a high variability in the timing of scission²⁷.

Deletion of coat proteins Sla2 and Ent1 results in a particular phenotype in which actin polymerization is achieved, but the membrane is decoupled from actin forces, resulting in actin “flames” without membrane bending^{32,37}. The complex between proteins Sla1, Pan1 and End3 links the early coat to other coat proteins and polymerized actin, is involved in actin regulation itself, and connects vesicles to actin cables and endosomes^{38–40}. The arrival of Sla1 is a strong predictor of successful endocytosis^{26,41}. These coat proteins are pulled upwards into the cytoplasm, and follow the moving membrane.

1.3.3.3 Actin module

Once the coat proteins are assembled, proteins that nucleate and organize the actin machinery are recruited. Actin filaments are nucleated by the Arp2/3 complex, and act in concert with other actin nucleation promoting factors (NPFs), such as the yeast WASP homologue Las17, type 1 myosins Myo3 and Myo5, Pan1, and actin binding protein Abp1. Apart from Pan1, which moves inwards upon membrane movement and forms part of the coat module, the remaining NPFs are recruited to the base of endocytic sites and do not move inwards with the membrane³⁴. Las17 is a potent actin nucleator, without which endocytosis essentially fails⁴². Myo3/5 are non-processive motors that interact with and can translocate actin filaments, but whose mechanistic contribution is unknown. Deletion of either Myo5 or Myo3 has subtle phenotypes, but deletion of both effectively blocked endocytosis⁴². Abp1 binds actin filaments and activates the Arp2/3 complex.

Bbc1, F-BAR protein Bzz1, and Vrp1 are other actin associated proteins that are recruited within the actin module. Bbc1 is known to inhibit Las17 NPF activity, its deletion accumulates actin at endocytic sites⁴³. Bzz1 relieves Las17 of NPF activity inhibition by Sla1⁴². Vrp1 stimulates the Arp2/3 complex, recruits myosins, and interacts with Las17^{44,45}.

Once NPFs and WASP/Myo proteins are recruited, Arp2/3 is recruited and actin polymerization begins. Along with Arp2/3, actin crosslinkers like Sac6 and Scp1, capping protein complexes like Cap1/Cap2, Aip1/Cofilin, Abp1/Aim3 are recruited. This begins the invagination of membrane, along with the coat proteins. Actin monomers are added at the base of the invagination, and coupled into the membrane via coat proteins, so as actin

polymerization progresses, the entire actin network is pushed upwards, taking the membrane along with it³⁴.

1.3.3.4 Scission module

While the role of the yeast dynamin-like Vps1 is unclear, relatively few copies of the Rvs complex are recruited in a time window that spans only a few seconds, and membrane scission occurs when the invagination is about 140nm long, indicating tight regulation of this transition^{30,34}. Coat proteins and the actin network are rapidly disassembled by phosphorylation and dephosphorylation of the components. What actually regulates scission in yeast is not yet determined (see 1.3.5).

1.3.4 Membrane scission in mammalian cells

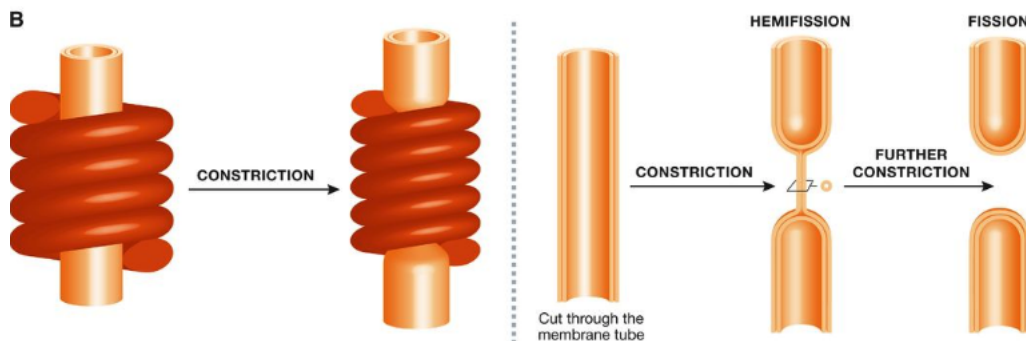
1.3.4.1 Scission is dependent on dynamin

In mammalian cells, membrane scission in endocytosis is primarily effected by the GTPase dynamin. Dynamin was discovered as a microtubule interacting protein⁴⁶, and since has been shown to have a pivotal role in membrane scission and fission at many different organelles across the cell. The importance of dynamin in endocytosis was demonstrated in a temperature sensitive mutant of the *Drosophila shibire* gene, which results in paralysis of flies at the non-permissive temperature. These flies fail to form synaptic vesicles^{47–49}. *Shibire* codes multiple isoforms of dynamin that are differentially expressed across the organism⁵⁰. Knock-down of dynamin isoforms results in initiation of clathrin-coated pits, but vesicle formation is disrupted, resulting in accumulation of a large number of long membrane tubes⁵¹.

1.3.4.2 Dynamin is an oligomeric GTPase

Dynamins consist of a GTPase domain, a stalk region, a bundle signalling element that acts as the linker between the GTPase domain and stalk, a PIP2-binding pleckstrin homology domain (PH) domain and a proline rich domain (PRD) that extends beyond the GTPase domain⁵². In-vitro, dynamin oligomerizes into helical structures with the PH domain apposed against the membrane, and the GTPase domain facing away from the membrane^{53,54}. Dynamin within the helical structure undergoes conformation changes upon GTP hydrolysis that constricts the helix as well as the membrane tube under it, collapsing the inner leaflet of the

bilayer membrane into a hemi-fused state, resulting in membrane fission⁵⁵. Disruption of its GTPase activity results in membrane tubes that accumulate dynamin, as well as the BAR domain proteins endophilin and amphiphysin^{56–58}



1.3.4.3 Dynamin interacts with BAR proteins to cause scission

Dynamin arrives at clathrin-coated pits via interaction with BAR proteins endophilin and amphiphysin⁵¹. BAR domain proteins form intrinsically curved protein dimers named for the conserved module contained in their founding members, metazoan BIN/ Amphiphysin and yeast proteins Rvs167, Rvs161. In addition to the BAR domain, most BAR proteins have additional motifs that mediate their interaction with membranes or other proteins: some BAR proteins have an N-terminal amphiphatic helix (N-helix) that is inserted into the membrane, phosphoinositide binding motifs like phox or pleckstrin homology (PH) domains direct BAR proteins to specific lipids within membranes, some BAR proteins have Src homology 3 (SH3) domains that mediate protein-protein interaction. These SH3 regions act as a scaffold for the proline-rich domains of dynamin 59.

1.3.4.4 Dynamin and BAR proteins interact via PRD and SH3 regions

Dynamin's PRD interacts with the SH3 domains of BAR proteins endophilin and amphiphysin^{59–62}. Endophilin recruitment is reduced in the absence of dynamin, and appears to inhibit the GTPase action of dynamin^{60,62,63}, while dynamin recruitment is decreased without endophilin. Amphiphysin levels are unchanged in absence of dynamin, while deletion of amphiphysin results in increased recruitment and prolonged lifetimes of dynamin and absence of membrane scission⁶⁰. These results suggest a role for amphiphysin for disassembly of dynamin involving GTP hydrolysis, and a role for endophilin in dynamin assembly,

although the mechanistic interplay between the two BAR proteins with dynamin is still debated, and the sequence of events is not clear^{63,64}. Dynamin localization to localize to clathrin-coated pits is not dependent on BAR proteins, but both GTP hydrolysis and interaction with BAR proteins is necessary for efficient vesicle scission^{60,65}.

1.3.5 Membrane scission in yeast

1.3.5.1 Yeast dynamin-like proteins

In yeast, three dynamin-like large GTPases have been identified: Vps1, Dnm1, and Mgm1. Dnm1 and Mgm1 are involved in mitochondrial fission and fusion⁶⁶. Vps1 is essential for vacuolar protein sorting⁶⁷, is involved in fission and fusion of vacuoles⁶⁸ and peroxisomes⁶⁹, is required for regulation of golgi to endosomal trafficking⁷⁰, and may arrive at early endocytic events⁷¹. None of the three yeast dynamins have the typical PH domain^{72,73} that in mammalian interacts with the lipid bilayer. Instead, an “InsertB” region likely performs the same function. Although yeast dynamins also do not have PRDs that could interact with the SH3 domains of yeast BAR proteins, Vps1 has been shown to interact with the clathrin and other endocytic proteins^{71,74,75}, though other work has failed to observe localization of Vps1 at endocytic sites^{41,74}. The role of Vps1 in endocytosis is not clear, but it is a candidate for the role of the canonical dynamin in CME.

1.3.5.2 Yeast BAR domain proteins Rvs161/167 regulate scission timing

In yeast, the Amphiphysin/ Endophilin homologue is the heterodimeric complex Rvs161/167⁷⁶ (Rvs), of which Rvs167 has an SH3 domain. Rvs arrives at endocytic sites in the last stage of the endocytosis, and disassembles rapidly at the time of membrane scission³⁴. Deletion of Rvs results in failure of membrane scission in nearly 30% of endocytic events²⁶. Scission failure is identified by the movement inwards of the plasma membrane into the cytoplasm, followed by its retraction back towards the cell wall, indicating a failure to form vesicles. No mutation of known endocytic proteins exhibits this phenotype, while some mutations like that of the yeast Syndapin Bzz1 and Synaptosomal Inp52, in the background of rvs Δ , exacerbates the retraction phenotype⁴¹. This unique profile suggests that although Rvs is not necessary for scission, localization of the complex

makes scission more efficient, and Rvs likely acts in concert with other proteins to effect this efficiency.

1.3.5.3 What causes scission?

How Rvs may affect scission has not been determined. Since yeast dynamins do not have a PRD, there is likely no interaction with Rvs, so a mechanism that does not involve PRD-SH3 interactions like in mammalian cells is likely necessary. Yeast cells are under high turgor pressure that makes forces from actin polymerization necessary for invagination^{77,78}. There is therefore likely to be some interplay between scission-stage proteins and the actin network that could modulate the final shape transitions.

Proposed scission mechanisms

Several scission models have been presented in the literature so far. Yeast dynamin is the obvious solution to membrane scission. Although none of the three dynamin-like proteins has a proline-rich domain, Vps1 has been suggested to play a role in endocytosis⁷¹. *vps1Δ rvs167Δ* double mutant has been shown to increase membrane retraction rates after invagination⁷⁹, an indication of scission failure. Another hypothesis has proposed that lipid hydrolysis by yeast synaptojanin-like proteins can cause vesicle scission⁸⁰. Synaptojanins dephosphorylate PIP2, a lipid subtype enriched at endocytic sites. In this model, Rvs would form a scaffold on the membrane tube, protecting the underlying PIP2 and causing a boundary between BAR-protected PIP2 at the tube and hydrolyzed PIP2 at the bud tip. This lipid boundary produces a line tension at the interphase that could generate enough force to pinch off a vesicle.

In-vitro experiments have proposed protein friction as a mechanism by which membrane scission could occur⁸¹. In this model, a BAR domain scaffold exerts a frictional force on a membrane that is pulled under it. Such a friction-dependent membrane scission model would predict that if more BAR proteins are added to the membrane, frictional force would increase, and scission should occur at shorter invagination lengths. *In-vivo*, this pulling force is generated by actin polymerization.

Recently, steric pressure exerted on the membrane by disordered protein domains that typically follow the BAR region has been proposed as a mechanism for scission⁸². In these experiments, the amphiphysin BAR domain is able to drive scission, but scission efficiency increases

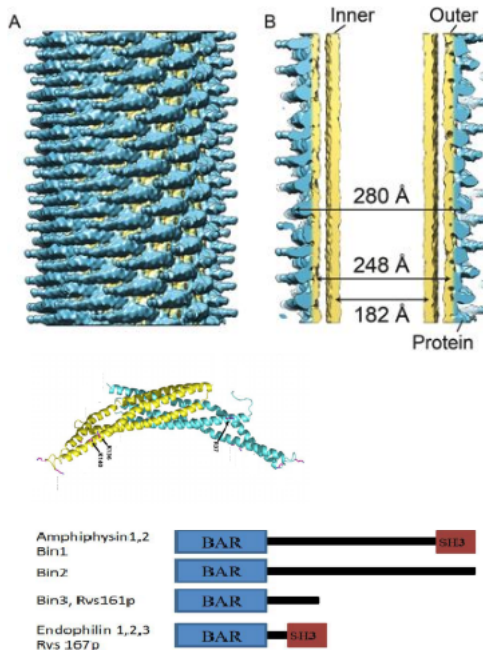
three to four-fold because of the disordered protein domains, and these domains do not need to have any specific biochemical properties: they can be replaced by any other disordered protein region. It has also been proposed that BAR domain scaffold membrane tubes and stabilize them, preventing scission^{83,84}. For a more detailed discussion on these models, see /refresults

Many of these theories are contradictory, based on in-vitro data, using mammalian BAR proteins, at concentrations of protein orders of magnitude higher than physiological levels, and without the context of interaction partners, relevant membrane tension, native lipid composition and intra-cellular turgor pressure: a mechanism for membrane scission in yeast is yet to be determined.

1.4 BAR domain proteins

The BAR protein superfamily have a highly conserved BAR domain structure across eukaryotes and are involved in a range of cellular processes including endocytosis, actin organization, cell polarity, transcription and tumor suppression^{85,86}. Of the mammalian isoforms of the founding members, Bin1 (Amphiphysin II) and Bin3 are ubiquitously expressed, while Amphiphysin I is expressed only in neurons. The conserved portion of these proteins, as well as of Rvs167 and Rvs161, is an N-terminal region that forms the BAR domain. This domain typically forms dimers with other BAR domains, and have an intrinsic curvature defined by the dimerization angle. This curvature categorizes BAR proteins to classical BAR, Fer-Cip4-homology-BAR (F-BAR, shallow curvature), and I-BAR (inverted curvature). Membrane-binding is mediated by cationic clusters that bind via non-specific electrostatic interactions to anionic lipids like phosphatidyl serine (PS) or phosphatidylinositol (4,5)-bisphosphate (PtdIns(4,5)P₂ „ henceforth PIP₂).

BAR dimers are able to oligomerize and scaffold large areas of membrane. These scaffolds can tubulate and generate curvature across membrane regions much larger than the dimensions of a BAR dimer^{62,87}. BAR scaffolds can also bind membranes in a curvature-dependent manner. Correlation between the membrane shapes that they bind in-vivo and their intrinsic curvature has been shown for many BAR proteins: they may induce, stabilize, or generate specific curvature within cells.



1.4.1 NBAR proteins and membrane shapes

Classical BAR domain proteins form a crescent-shaped structure. Some of them have an N-terminal amphiphatic helix (N-helix), forming a subclass of classical BAR called NBAR domains. The two significant endocytic BAR proteins, Endophilins and Amphiphysins, are NBAR proteins. The 35-40 residue N-helix acts as an amphiphatic wedge that is unstructured until it is inserted into the upper leaflet of a membrane bilayer⁸⁷. The insertion causes displacement of lipids, resulting in bending of the membrane, indicating that N-helix insertion into a membrane bilayer could favor membrane scission both energetically and kinetically^{84,88}. BAR domains lacking this helix are not able to efficiently tubulate vesicles⁸⁹. The N-helix also increases efficiency of binding to liposomes⁶² in a curvature sensitive manner, and confers salt sensitivity⁸⁹.

High resolution structural data has shown that NBAR proteins can hold form helical scaffolds on tubular membranes^{87,90,91}. An energetically favorable arrangement of BAR domains consist of dimers parallel to each other, apposed to the membrane, supporting membrane tubulation and preventing scission by stabilizing the membrane tube⁸⁴. Hybrid N-helix and BAR scaffolds can therefore allow coexistence of both vesicles and tubules, with preference for one or the other depending on the ratio between number of N-helices that favor vesiculation, and BAR generated scaffold stability⁸⁴.

Both BAR proteins implicated in CME , Amphiphysin and Endophilin are shown to tubulate membranes in-vitro^{87,89,91} and form a helical scaffold. The tubulation diameter resembles the diameter of the proteins themselves, and involve lateral interactions of the neighboring BAR domains⁹². Both BAR domains are able to form mixed helices in the presence of dynamin^{62,93}.

1.4.2 NBAR protein in endocytosis: Amphiphysin

Two mammalian isoforms of Amphiphysins (Amph) are found. AmphI is enriched in neurons in mammals, while AmphII (Bin1) is expressed in other tissue types, with one isoform enriched in muscle T-tubule junctions⁹⁴. The only Amphiphysin (d-Amph) in flies is expressed in various tissues, and enriched at muscle T-tubule junctions in flies. The d-Amph dimer forms a coiled coil, with each BAR domain made of three long, kinked alpha-helices⁸⁷. In-vitro, liposome tubulation activity of Amphiphysin is concentration dependent, at very high concentrations, it is also able to sever tubular membrane to form vesicles⁸⁷.

Amph I and II both have BAR domains, a proline rich region, and C-terminal SH3 domain. Amphiphysin I, but likely not II binds Clathrin and its adaptors⁹⁵ and can polymerize clathrin into invaginated lattices in a BAR domain dependent manner⁸⁷, while both bind dynamin, and the lipid phosphatase Synaptjanin⁶¹.

1.4.3 NBAR protein in endocytosis: Endophilin

Endophilins A1-A3 (EndoA) were discovered as SH3 domain containing proteins⁹⁶ that co-localized with dynamin, and interacted with Synaptjanin⁵⁸ and amphiphysin⁹⁷: all already identified as important regulators of synaptic vesicle recycling by endocytosis. A second mammalian protein was later discovered as related, and then termed EndophilinB (EndoB). Other sequenced eukaryotes have a single isoform of EndoA and B.

EndoA1-3 isoforms are found in neurons, ubiquitously, and enriched in the brain and testes respectively. All three are found at presynaptic membranes. Crystal structure of EndoA1 shows essentially the same structure as that of amphiphysin, with an additional amphiphatic helix similar to the N-helix, located at the centre of the crescent-shaped dimer^{89,98}. This helix is thought to insert into the membrane in the same way as the

N-helix, potentially inducing faster tubulation of membranes. EndoA1 and 2 may interact with calcium channels at synapses, and may be involved in lipid modification^{99,100}, suggesting different roles for the two BAR domain proteins in membrane interaction. Endophilin interacts with dynamin, NWASP and Synaptosomal-associated protein of 105 kDa (Synaptosomal-associated protein of 105 kDa) proteins via its SH3 domain^{61,63,101}.

1.4.4 NBAR protein in yeast endocytosis: the Rvs complex

RVS167 and RVS161 (reduced viability upon starvation) genes were discovered in a screen that tested for survival under starvation conditions¹⁰². Rvs167 and Rvs161 are both NBAR domain proteins that thought to form obligate heterodimeric complexes (Rvs) in-vivo^{103,104}. Although there is evidence of heterodimerization: loss of one destabilizes the other, deletion phenotypes of Rvs167 is the same as that of Rvs161, and FCCS measurements indicate that they dimerize^{26,103,105}, it has also been reported that Rvs161 has some functions that do not match that of Rvs167. Rvs161 for instance, interacts with Fus2 in cell-cell fusion, while Rvs167 does not¹⁰⁶. It is consistent however, that at endocytic sites they function together as heterodimers.

Rvs161 and Rvs167 are similar in structure at the N-terminus, both contain NBAR domains that are 42% similar, and although share 21% identity, are not interchangeable¹⁰⁷. In addition to the BAR domain, Rvs167 has a Glycine-Proline-Alanine rich (GPA) region and a C-terminal SH3 region. The GPA region is thought to act as a linker with no known other function, while loss of the SH3 domain affects budding pattern and actin morphology. Most Rvs deletion phenotypes can however, be recapitulated by expression of the BAR domain alone¹⁰⁴, suggesting that the BAR domains are the main functional unit of the complex.

Deletion of the genes show abnormal actin morphology, confer salt sensitivity, as well as amino-acid and lipid sensitivity, and have abnormal budding pattern^{103,108–110}. Homology modelling has shown that the BAR domain of Rvs167 is similar to Amphiphysin and Endophilin, and is therefore also likely to function similarly to the mammalian homologues. In keeping with this theory, Rvs has been shown to tubulate liposomes in-vitro¹¹¹.

Averaged centroid tracking of the Rvs complex has shown that Rvs arrives in the scission stage of endocytosis. When maximum number of

Rvs is recruited, that is, at peak fluorescent intensity, the centroid jumps inwards, concomitant with a sharp decay in fluorescent intensity. This behavior is unique among endocytic proteins, and since similarity in structure with Amphiphysin/ Endophilin BAR domains is expected, has led to the proposition that Rvs may also form a helical scaffold on the membrane tube, whose sudden disassembly either leads to or is caused by membrane scission. The sharp movement into the cytoplasm of the Rvs centroid is then caused by the disassembly of the scaffold, and a jump in the centroid position to the remaining Rvs on the base of the newly formed vesicle³⁴. How Rvs is recruited to endocytic sites, and the cause of the scaffold disassembly are not known, and are the major questions addressed in this work.

2 | Aims of the study

More than 50 different proteins are involved in clathrin-mediated endocytosis. At endocytic sites, they assemble into a small, complex and dynamic macromolecular machinery. Although individual components have been identified and well-characterized during decades of research, their structural organization is poorly understood. In my PhD project, I proposed that single-molecule localization based superresolution microscopy provides both the molecular specificity and necessary spatial resolution to study how proteins are arranged *in situ* within the endocytic machinery. More specifically, I addressed the following questions:

- How is Rvs recruited to endocytic sites?

The recently developed technique of localization microscopy critically depends on dense and specific fluorescent labeling of the cellular structure of interest with a dye suitable for localization microscopy. In the first part of my project, I established an optimized sample preparation pipeline to enable high quality dual-color localization microscopy of yeast cells. These efforts are described in section ??.

- How does it regulate scission

3 | Results

3.1 Rvs localization in yeast endocytosis

Averaged centroid tracking, as described in Picco et al., can quantify the movement and dynamics of endocytic proteins along the timeline of membrane invagination and scission. Briefly described, yeast cells expressing fluorescently-tagged endocytic proteins are imaged at the equatorial plane. Since membrane invagination progresses perpendicularly to the plane of the plasma membrane, proteins that move inward with membrane ingress now do so in the imaging plane. Centroids of many endocytic patches, for example, containing Sla1-GFP, are thus tracked. Since yeast endocytic sites show highly stereotypic behavior, the centroids of the proteins involved can be averaged as they arrive at and depart from the plasma membrane, leading to an averaged centroid tracked with high spatial and temporal resolution. When different endocytic proteins are simultaneously imaged with the abundant actin binding protein Abp1, Abp1 provides a frame of reference to which the other proteins can be now aligned.

Centroid tracking shows that the late-stage coat protein Sla1 arrives and accumulates at endocytic sites, starts to moves into the cytoplasm at the onset of actin polymerization 1,2. Sla1 moves into the cytoplasm along with the membrane and follows its movement during endocytosis. In WT cells, Sla1 moves about 140nm into the cytoplasm, at which point vesicle scission occurs. It will be used throughout this work as the marker for membrane movement. As inward movement of the membrane begins, the Sla1 coat is disassembled, inferred from the decay of the fluorescent intensity of Sla1-GFP 2, shown in 3.1. As has been shown before, Rvs localizes to endocytic patches at the yeast plasma membrane in the late scission-stage1,2. Rvs167 arrives after a parallel membrane tube is formed, and scission occurs at 60% of its lifetime at the plasma membrane1,3.

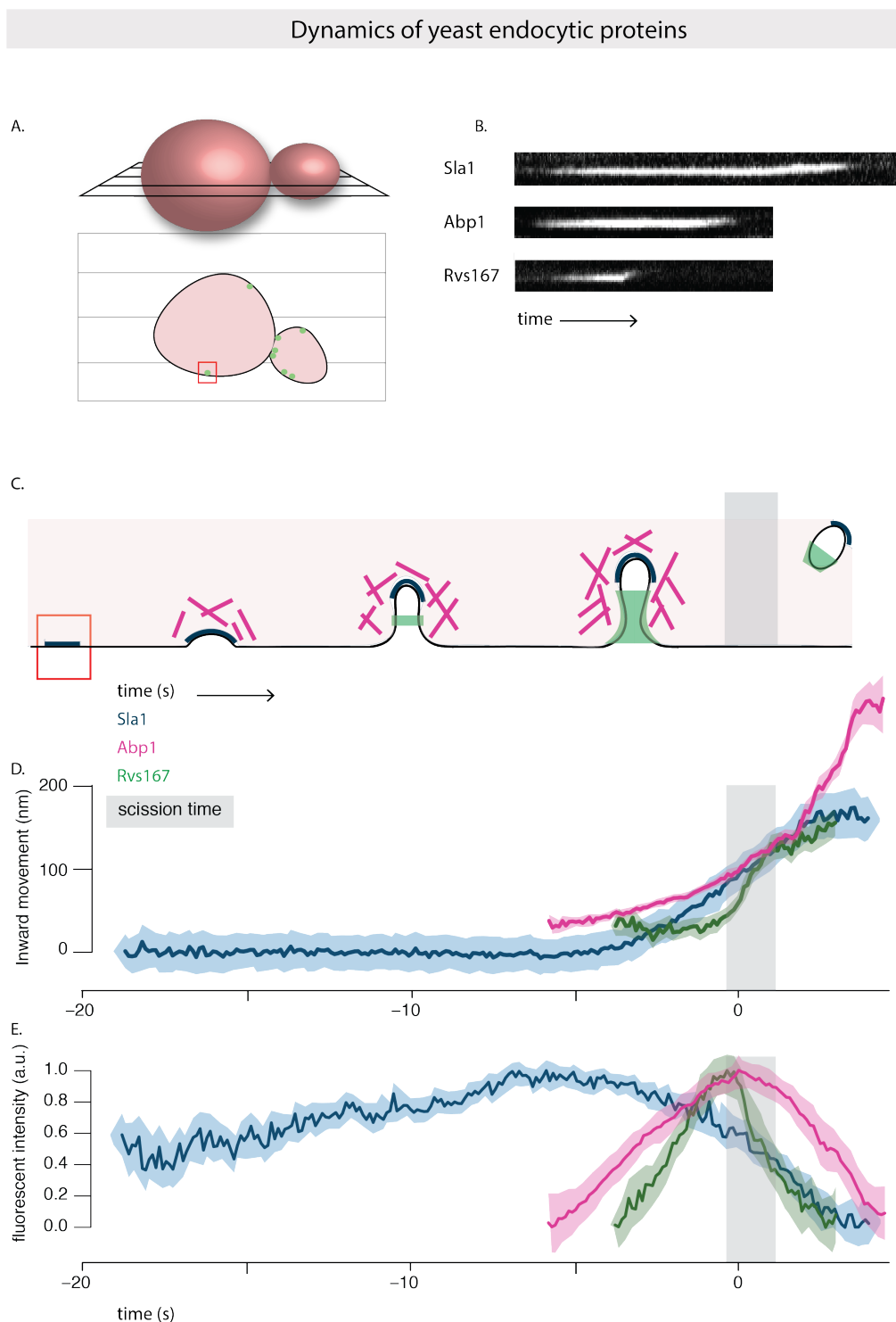


Figure 3.1: 1A: Above: Schematic of a yeast cell, showing the equatorial plane. Below: Cross section of the cell at the equatorial plane, with fluorescently tagged endocytic proteins at the plasma membrane. B: Kymographs of Sla1-GFP and Rvs167-GFP at endocytic patches at the plasma membrane. Movement of coat protein Sla1-GFP shows slow inward movement, while Rvs167-GFP shows a sharp jump into the cytoplasm that is concomitant with membrane scission and vesicle formation. Exposure rate for kymograph, 80ms. C: Schematic of the timeline of membrane invagination during endocytosis, with Sla1, Abp1 and Rvs167 indicated. D, E: Movement and normalized fluorescent intensity of Sla1, Abp1 and Rvs167 during endocytosis. Sla1 follows the membrane as it moves into the cytoplasm. Rvs arrives at membrane tubes, potentially forming a scaffold. At scission, the scaffold along the tube is disassembled, resulting in an inward jump of the Rvs167 centroid, to protein localized at the base of the newly formed vesicle, and a sharp decay in fluorescent intensity. Abp1 intensity drops after membrane scission. D and E are aligned in so that time=0 (sec) corresponds to scission time.

At the time of scission, the Rvs167-GFP centroid shows a sharp jump into the cytoplasm, a profile that is unique among endocytic proteins. Concomitantly, fluorescent intensity of Rvs167-GFP shows a sudden decay. Abp1 is used throughout this work as a marker for the actin network. Abp1 intensity also peaks at scission time, and drops after scission, indicating disassembly of the actin network upon vesicle formation. Thus, in WT cells, fluorescence intensity of Abp1 and Rvs167 begin to drop at the same time. Henceforth, unless indicated, "scission time", or time=0 (s) refers to the time at which fluorescent intensity of averaged Abp1 patches peaks. The other endocytic proteins are aligned in this timeline as described by Picco et al., by simultaneous dual-color imaging of the respective proteins with Abp1. The movement away from the plasma membrane of the averaged centroid of a protein is referred to as "movement". Averaged centroids for different GFP-tagged proteins are obtained from tracking 30-50 endocytic patches in 10-15 yeast cells.

3.2 Rvs deletion phenotype

The Rvs complex, as has been discussed in section 1, influences efficiency of membrane scission. Recruitment in the final stage of membrane movement, localization to the membrane tube, and disassembly concomitant with scission all indicate that Rvs could mechanistically influence the scission process. In order to quantify this influence, I tracked Sla1-GFP in *rvs167Δ* cells and compared its movement against WT Sla1-GFP. Rvs167 and Rvs161 are obligate heterodimers at endocytic sites, and deletion of one of them is expected to result in the loss of the other during endocytosis. Movement of Sla1 is reduced in *rvs167Δ* to about 60nm instead of the 140nm seen in WT cells. CLEM studies have shown that Rvs167 only localizes to endocytic sites after the tubes are 60nm long: membrane invagination is unaffected in *rvs167Δ* cells till the expected time of arrival of Rvs, after which membrane scission occurs, rather than further invagination. This indicates that first, membrane scission can occur at invagination lengths of 60nm. Then, that the arrival of Rvs prevents membrane scission at this point and allows further membrane invagination.

3.3 Recruitment of Rvs and function of domains

BAR domains: curvature sensing or generating? Cellular membrane shape is a result of properties like rigidity, tension, intracellular pressure,

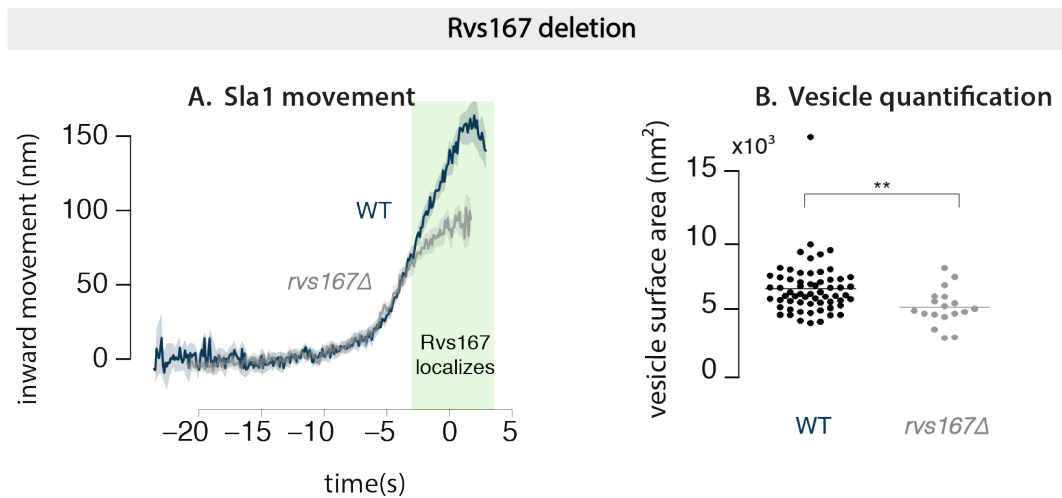


Figure 3.2: A: Averaged centroid movement of Sla1-GFP in WT and *rvs167 Δ* cells. Time=0 (s) for WT Sla1 is scission time. *rvs167 Δ* Sla1 is shifted to move at the same time as WT B: Vesicle surface area for WT and *rvs167 Δ* determined by CLEM. Data used with permission from Wanda Kukulski.

that are all influenced by membrane lipid composition and the proteins embedded in it^{1,2}. Since tension, pressure, and rigidity all oppose membrane deformation, energy is required to deform and bend it. BAR domains can generate curvature if the energy required to deform the membrane is less than the energy spent in binding flat membrane.

Curvature-generation by scaffolding and imposing its own shape on membranes has been extended to various types of BAR proteins, (Arkhipov et al., 2009; Frost et al., 2008; Henne et al., 2007; Itoh et al., 2005; Pykalainen et al., 2011; Saarikangas et al., 2009; Shimada et al., 2007; Yu and Schulten, 2013). In order for BAR scaffolds to impose membrane curvature, some requirement have to be met³: they have to have present a large membrane-interacting surface that can mediate membrane binding, have intrinsic curvature that can be imposed on the surface, and have a rigid structure that can overcome bending resistance of the membrane. Because of their shape (Peter 2004, Gallop 2006, Weissenhorn 2005), and their capacity to oligomerize into large assemblies on tubes (Mim 2012, Mizuno 2010, Takei 1999, Yin 2009), it has been suggested that BAR domains impose their shape on the membrane, and generate membrane curvature on cellular membranes. Further, it has been shown that the central BAR region is rigid and required for tubulation, both in-vivo and of liposomes⁴. The N-helix of NBAR domains can also generate curvature independently of the BAR scaffold (Varkey 2010, Westphal and Chandra 2013). In endophilin, the BAR domain is relatively far from the membrane,

suggesting a mechanism dependent on the N-helix (Jao 2010). Different BAR domains thus likely employ different mechanisms to interact with the membrane for generating vesicles, and tubes (Ambroso 2014). For example, the N-helix of endophilin is necessary for liposome binding⁵, while that of amphiphysin is important, but not necessary⁶.

Curved BAR proteins that can induce curvature are also able to sense curvature: *in-vitro*, BAR domains show a preferential-binding to vesicles based on their intrinsic curvature. Curvature-generation and sensing seem to intrinsically coupled mechanisms. That BAR domains are able to generate curvature does not imply that this is their function, at least in endocytosis: *in-vivo*, the significance of curvature-generation is not determined. Tracking over thirty different endocytic proteins in NIH-3TC cells (derived from mouse fibroblasts), TIRF imaging shows that Endophilin2 and Amphiphysin1 arrive late in the endocytic time-line right before scission⁷, suggesting they arrive when membrane tubes are already formed.

In the case of Rvs, as has been shown earlier, and seen in 3.2, the Rvs complex localizes to sites late in the endocytic timeline, close to scission⁸. CLEM studies have further shown that Rvs localizes to sites after the membrane invaginations are about 60nm deep into the cytoplasm: Rvs localizes once membrane curvature is established. Whether this localization is dependent on membrane curvature, recognized by the BAR domain has not been shown.

3.3.1 BAR domain senses membrane curvature *in-vivo*

To test whether Rvs is recruited because of membrane curvature, I first imaged Rvs167-GFP without the BAR domain, that is Rvs167-delsh3-GFP (henceforth referred to as BAR). BAR-GFP forms cortical patches 3.3, so the BAR domain is able to localize to the plasma membrane in the absence of the SH3 domain. In a yeast strain expressing both BAR-GFP and Abp1-mCherry, BAR-GFP co-localizes with Abp1, indicating that BAR domains are recruited to endocytic patches 3.3). In order to test whether this localization is due of membrane curvature, I compared the dynamics of Rvs167-GFP against BAR-GFP in *sla2Δ* cells 3.3 (D-F). Sla2 is a coat protein that acts as a linker between the membrane and the actin cytoskeleton by binding both via its N-terminal ANTH domain, and its

C-terminal THATCH domain. This allows forces generated within the actin network to be transmitted to the membrane¹¹. In *sla2* Δ cells, rather than cortical actin patches, an “uncoupling phenotype” is observed^{11,12}. Although endocytic coats are formed, actin is polymerized continuously at these sites, the membrane is not pulled inwards, and vesicles are not formed: forces generated by the actin network are not transmitted to the membrane (3.3 D-F).

In *sla2* Δ cells, Rvs167-GFP is recruited to the plasma membrane 3.3 at the plasma membrane, and together with Abp1-mCherry. Some Rvs167-GFP patches persist at the plasma membrane, while many are assembled and disassembled at Abp1 patches. Some Rvs167 patches do not co-localize with Abp1. In *sla2* Δ cells expressing BAR-GFP, localization is mostly removed except for rare transient patches at the plasma membrane that are co-localized with Abp1, while most of the patches appear to be recruited independent of Abp1. Rvs167-GFP and BAR-GFP patches are both dynamic, indicating an interaction exists in both cases that is able to assemble and disassemble Rvs patches at the plasma membrane.

3.3.2 The SH3 domain is able to localize Rvs in an actin and curvature-independent manner

As I show in the previous section, full-length Rvs is able to localize to cortical patches in *sla2* Δ cells. This localization must come from the SH3 domain, since BAR alone does not localize in cells without *sla2*. We expected that the SH3 domain must interact with WASP or actin-binding proteins: an interaction with Abp1 has been shown, as well as with Las17, type I Myosins, and Vrp1. In order to prove this, I imaged BAR-GFP and Abp1-mCherry in *sla2* Δ cells treated with the actin sequestering agent LatrunculinA (LatA). LatA is a sea-sponge toxin that binds monomeric actin and prevents incorporation of actin into filaments. Since high actin turnover is required at endocytic sites, LatA effectively disassembles WASP components and other actin-binding proteins of the endocytic machinery, and blocks endocytosis. In combination with the *sla2* deletion, latA treatment will effectively prevent membrane curvature as well as remove actin-binding proteins from endocytic sites. Loss of actin binding proteins is verified by the loss of Abp1 signal in the RFP channel.

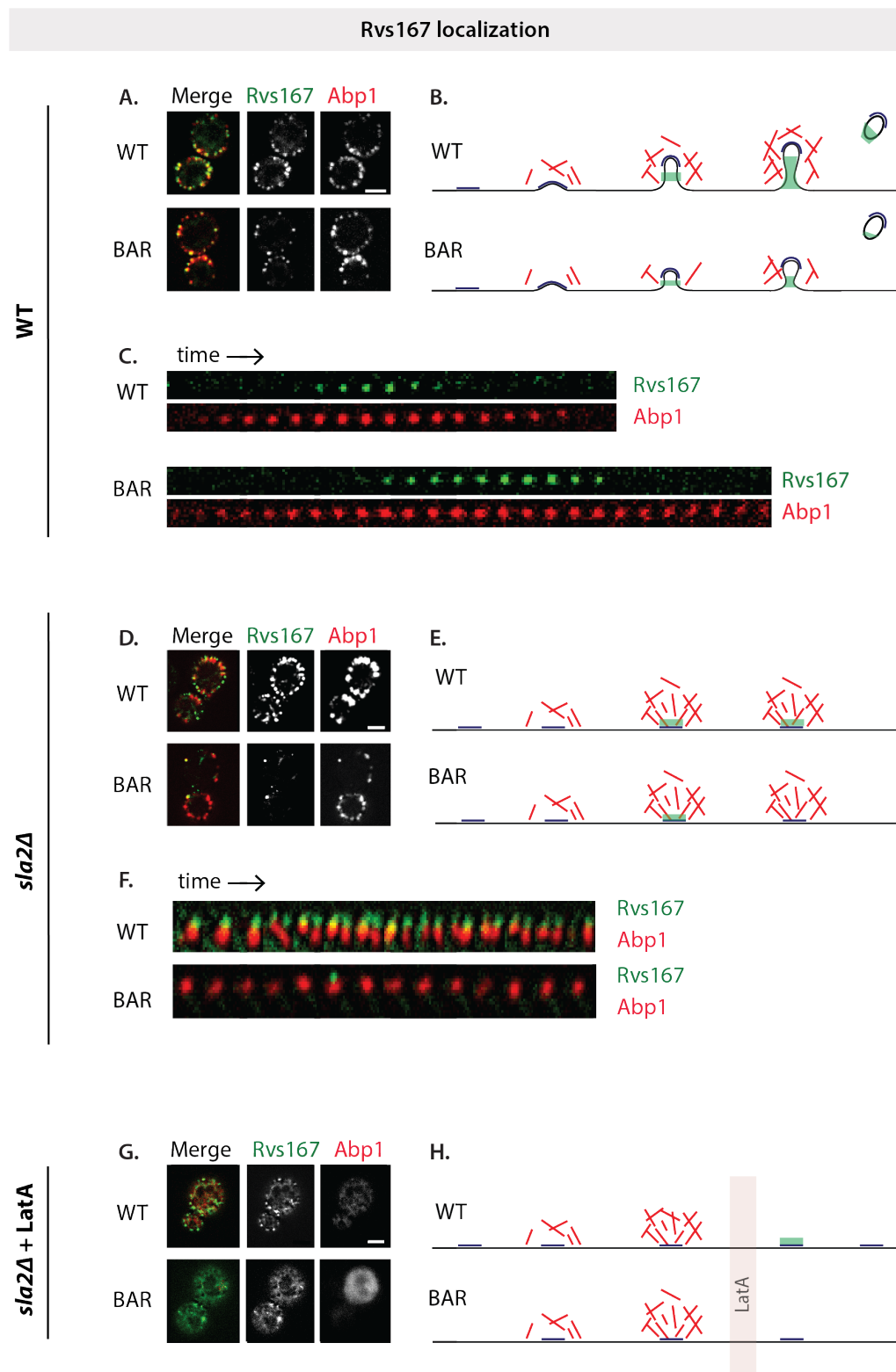


Figure 3.3: A: Max. intensity projections of time-lapse images of cells expressing GFP-tagged full length (FL) Rvs167 or BAR with Abp1-mCherry. Exposure rate 250ms. B: Schematic of endocytic progression in WT and BAR cells (see section 3.3.3). C: Montage of Rvs167-GFP and Abp1-mCherry at the plasma membrane in WT and BAR cells . Each frame of montage is every third frame of time-lapse images from A. D: Max. intensity projection of time-lapse images of *sla2Δ* cells expressing GFP-tagged FL or BAR Rvs167 and Abp1-mCherry. E: Schematic of membrane invagination in *sla2Δ* cells. F: Montage of GFP tagged FL and BAR Rvs167, and Abp1-mCherry. Exposure rate 1000ms for GFP, 800ms for RFP. G: Max. intensity projection of time-lapse images of *sla2Δ* cells of GFP-FL or BAR Rvs167 and Abp1-mCherry, after treatment with LatA for 10'. Exposure rate 1000ms for GFP, 800ms for RFP. H: Schematic of membrane invagination in *sla2Δ* cells treated with LatA. All scale bars = 2um.

Surprisingly, full-length Rvs is transiently localized to the plasma membrane in spite of the LatA treatment, suggesting that the SH3 domain is able to recruit Rvs to the plasma membrane. This recruitment occurs in the absence of a BAR-membrane interaction, since BAR-GFP localization is completely removed in LatA treated cells. Rvs167-GFP patches are transient, so an assembly-disassembly mechanism is mediated by the SH3 domain outside of its BAR domain interaction. Localization of Rvs161, which does not have an SH3 domain, is also removed by LatA treatment¹², supporting the conclusion that the BAR domains of the Rvs complex senses membrane curvature in-vivo.

3.3.3 Loss of the SH3 domain affects progression of endocytic sites

Since the Rvs167 SH3 domain plays a surprisingly large role in the function of Rvs, I investigated its effect further. SH3 domains are known to mediate protein-protein interaction by binding to proline-rich sequences that contain a core PXXP motif^{13,14} (where X is any amino acid). These domains are ubiquitous in cellular interaction pathways, and several endocytic proteins have at least one SH3 domain, found to self-regulate activity, as well as to modulate local concentrations of protein. Although SH3 domains are abundant, they appear to have specific binding partners. For the Rvs167 SH3 domain, neither the specific binding partner, nor its function in the scheme of endocytosis is known. From early work, the BAR domain is expected to act as the functional module of the Rvs proteins: most of the phenotypes of Rvs deletion can be compensated by expression of the BAR domain alone, although the SH3 domain is required in addition to the BAR domain for bipolar budding pattern¹⁵.

In order to probe the contribution of the Rvs167 SH3 domain to endocytosis, I studied membrane and scission dynamics by expressing Rvs167 without the SH3 domain (that is, BAR domain). Sla1 moves inwards to a maximum of approximately 50nm instead of the 140nm found in WT invaginations. Shorter invaginations with a maximum length of 60nm have been observed in the case of Rvs167 deletion by CLEM 10, which is approximately the same length as those observed in the BAR cells: loss of the SH3 domain appears to be detrimental to the function of the Rvs complex. That reduced inward movement of the coat seen in centroid tracking reflects membrane scission at shorter invagination lengths is confirmed by

CLEM on strains expressing Rvs167-GFP and Abp1-mCherry in WT and BAR strains (Fig.3.4E). Upon preliminary analysis, invagination lengths measured in the BAR strain are distributed around xxxxxxxxxxxxxxxxx

Quantification of the number of BAR-GFP molecules recruited to endocytic sites shows that without the SH3 domain, recruitment is reduced by half: the maximum numbers of BAR-GFP recruited is 50% of WT, at 57 +/- 9.9 molecules, compared to 113.5 +/- 5.2, although the cytoplasmic concentration of protein is not affected compared to Rvs167-GFP (see methods). Movement of Rvs167-GFP into the cytoplasm at scission time is reduced in BAR cells, and 10.4% of Rvs167 patches remain on the plasma membrane and are disassembled without inward movement, compared to only 2.56% in WT. Abp1-GFP recruitment without the SH3 domain is similarly reduced to 65% of WT recruitment, from a maximum number of 459.5 +/- 19.9 molecules in BAR to 302.9 +/- 12.9 in WT.

For a more detailed inquiry into changes in the endocytic machinery without the Rvs167 SH3 domain, I quantified the lifetimes of Rvs, and coat and actin network using Sla1 and Abp1 as markers in BAR cells using total internal reflection fluorescence (TIRF) microscopy. Unlike epifluorescence microscopy at the equatorial plane, which has been the method used for quantification so far, when using TIRF, only fluorophores up to a depth of about 100nm from the glass-sample interphase are excited. This reduces fluorescent signal from the cytoplasm, allowing detection of low intensity fluorescent signal, and is a better method for visualizing the early incidence of a protein at the plasma membrane than epifluorescence microscopy. Arrival of Rvs167-GFP, coexpressed with either Sla1-mCherry or Abp1-mCherry in BAR and WT cells are compared.

While the lifetimes of Rvs167 in WT and BAR are similar, as are Sla1 lifetimes in both cell types, there is a significant increase in the lifetime of Abp1 lifetime in BAR cells (not shown). I looked for differences in the timing of recruitment of endocytic proteins by looking at the difference in time between recruitment of Sla1 and Rvs167, and the difference in time between recruitment of Abp1 and Rvs in the WT and BAR cells. The time difference between recruitment of Sla1 and Rvs167 is unchanged between WT and BAR cells, while the difference in time between recruitment of Abp1 and Rvs167 is increased in BAR cells (Fig.??D).

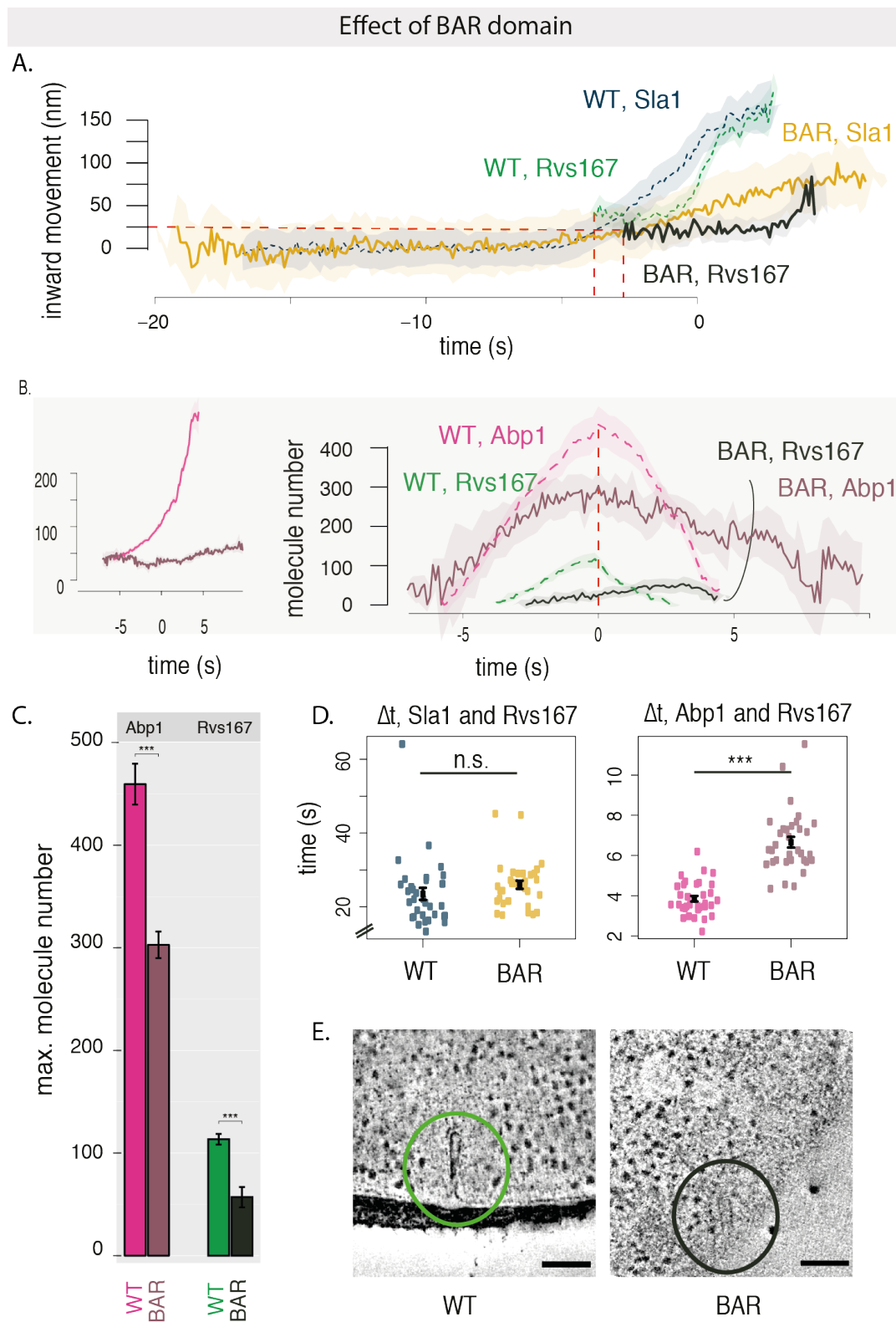


Figure 3.4: A: Movement of Sla1 and Rvs167 in WT and BAR strains. Centroids are aligned in time so that time=0 corresponds to the Abp1-mCherry fluorescent intensity peak in simultaneous dual-color imaging of the corresponding strains. C: Maximum number of molecule of Abp1-GFP in WT, and BAR cells, and Rvs167-GFP in WT and BAR cells, with standard error of mean. p values from a two-sided z test, * = $p \leq 0.05$, ** = $p \leq 0.01$, *** = $p \leq 0.001$. D: Difference in time between arrival of Sla1-mCherry and Rvs167-GFP, and Abp1-mCherry and Rvs167-GFP in WT and BAR strains. Exposure 560ms for each channel. Mean and standard error of the mean are shown, * = $p \leq 0.05$, ** = $p \leq 0.01$, *** = $p \leq 0.001$. p values of two-sided t test. E: Invagination lengths in WT and BAR cells measured by CLEM in cells expressing Rvs167-GFP and Abp1-mCherry.

3.4 Scission mechanisms

3.4.1 Yeast dynamin Vps1

Yeast dynamin is the obvious solution to membrane scission. Although none of the three dynamin-like proteins has a proline-rich domain, one of the yeast dynamins, Vps1 has been suggested to be involved in endocytosis^{11,12}. Rooij et al., suggest that Vps1 localizes to endocytic sites in the late scission stage, and that the *vps1Δ rvs167Δ* double mutant increases membrane retraction rates after invagination, an indication of scission failure. Vps1-GFP does not localize to endocytic sites in Gadila et al.¹³, but localizes to the golgi body and to vacuoles. Kishimoto et al. do not find a colocalization between Vps1 and Abp1 localization, and also report that the *vps1Δ rvs167Δ* double mutation does not affect membrane retraction rates. Vps1 tagged with both GFP as well as superfolded GFP, and imaged by TIRF microscopy fails to colocalize with Abp1 (data not shown, personal communication with Andrea Picco). The debate concerning the involvement of Vps1 in membrane scission in yeast has been compounded by the possibility that the GFP tag at the Vps1 C-terminal could interfere with its localization to endocytic sites, or its interaction with the Rvs complex.

3.4.1.1 Membrane scission is not dependent on Vps1

In order to exclude the possibility of interference from the GFP tag, I investigated the role of Vps1 by studying coat and scission proteins in *vps1Δ* cells. Movement of Sla1 and Rvs167 *vps1Δ* is compared against that in WT cells.

vps1Δ cells exhibit a growth defect at 37C, as has been reported¹¹. Sla1-GFP accumulates at the plasma membrane, moves inwards, and disassembles like in WT, as seen in the kymograph in 3.5. In WT cells, Sla1 moves into the cytoplasm about 140nm before membrane scission occurs. If Vps1 was required for membrane scission, Sla1 would be expected to undergo delayed or failed scission. However, *vps1Δ* does not increase the rate of membrane retraction. Inward movement of Sla1 is also not changed: it moves inward at the same rate, and to similar maximum of 140nm. Further, the averaged centroid of Rvs167 would not show the sharp jump into the cytoplasm if scission failed. If scission was delayed,

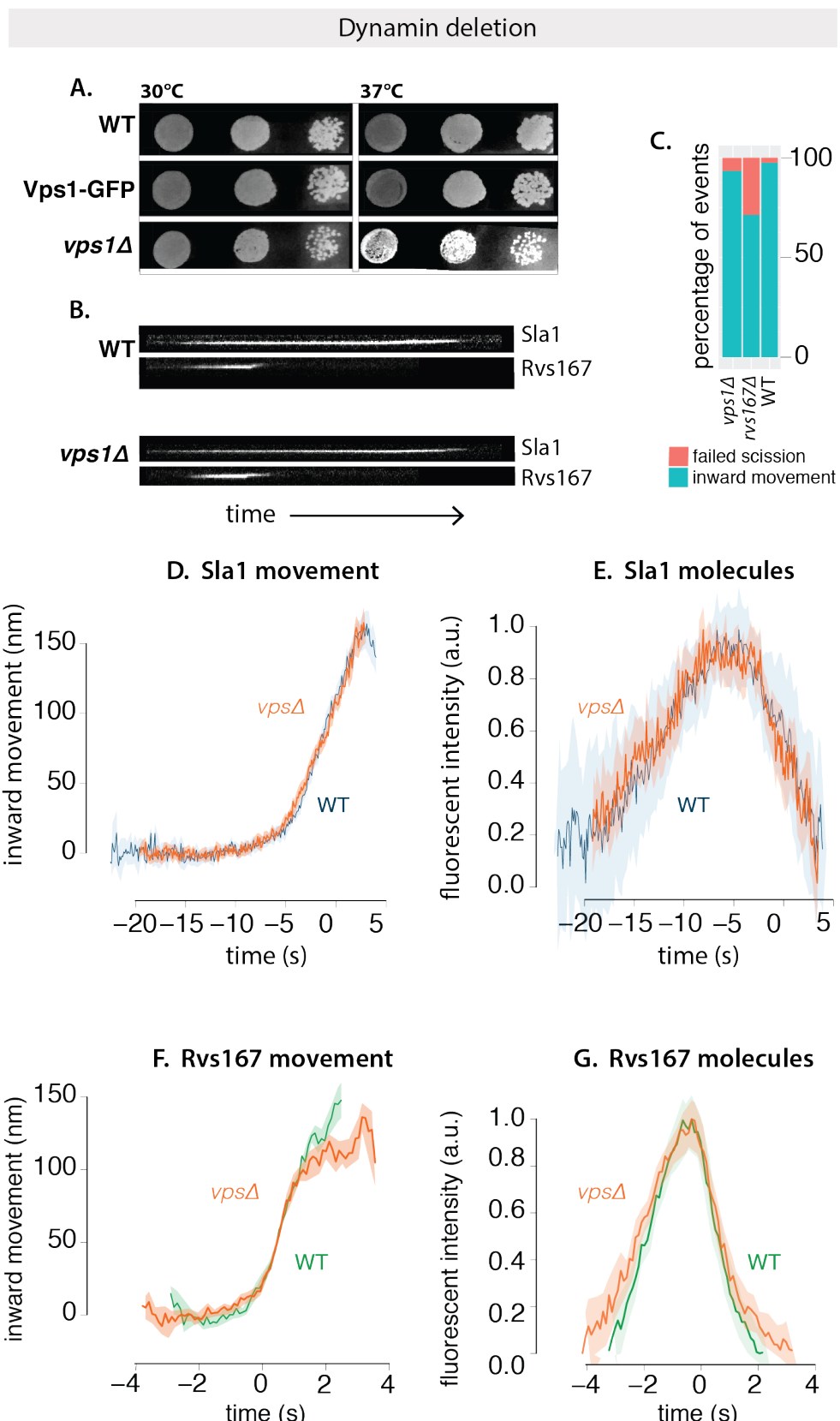


Figure 3.5: A: Dot spots of WT, Vps1-GFP, and *vps1Δ* cells at 30C and 37C. B: Kymographs of Sla1-GFP and Rvs167-GFP in WT and *vps1Δ*. Exposure 80ms. C: Failure rate of membrane scission, measured from retractions of Sla1, or lack of movement. D, E: Movement and normalized fluorescent intensity of Sla1-GFP in WT and *vps1Δ* cells. Time =0 (s) for WT Sla1 indicates scission time. *vps1Δ* Sla1 is shifted to move inwards at the same time as WT. F, G: Movement and normalized fluorescent intensity of Rvs167-GFP in WT and *vps1Δ* strains. Time =0 (s) for WT Rvs167 indicates scission time. *vps1Δ* Rvs167 is shifted so that fluorescent intensity maxima is at time=0 (s).

the average lifetime of Rvs167 would increase. The inward movement of Rvs167, and its average lifetime, however, remains the same as in WT. I conclude that if Vps1 does localize to endocytic patches in *S.cerevisiae*, it is not involved in regulating membrane scission.

3.4.2 Lipid hydrolysis and membrane scission

Another hypothesis has proposed that regulated lipid hydrolysis can cause vesicle scission¹⁹. Phosphatidylinositol (PIs) and their derivatives play important roles in many cellular processes including membrane trafficking and cell signalling. Conversion between lipid types is driven by kinases, lipases, and phosphatases and controlled throughout the membrane trafficking pathway.

Phosphatidylinositol(4,5)-biphosphate (PI (4,5) P₂) is an important lipid type found at the cell surface, and is enriched and depleted from endocytic sites at the plasma membrane in concert with the assembly and disassembly of the endocytic machinery. Synaptojanins form a subset of inositol polyphosphate 5-phosphatases that hydrolyze PI(4,5)P₂ to PI(4)P by removing the phosphate at the 5' position of the inositol ring, and play a role in CME and intracellular signalling, as well as in modulating the actin cytoskeleton¹⁴. Synaptojanins localize to endocytic sites, and in mammalian cells, disruption of Synaptojanin genes results in cellular accumulation of PI(4,5)P₂ and coated vesicles at the plasma membrane, suggesting a role for lipid hydrolysis in releasing coat proteins from nascent vesicles. Syaptojanins contain an N-terminal homology domain with the cytoplasmic domain of the yeast SAC1 gene, that is implicated in lipid metabolism, actin morphology, and vesicle transport in the secretory pathway¹⁵. A central catalytic domain is followed by a proline-rich C-terminal regions that are the canonical interaction partners of SH3 domains: they are known to interact with actin binding proteins and BAR domain proteins, potentiating also a role in membrane invagination and scission.

The yeast encodes three Synaptojanin-like proteins- Inp51, Inp52 and Inp53- that regulate phospholipid metabolism. Double deletion of Inp51 and Inp52 has been shown to increase the lifetime of endocytic proteins and produce aberrant membrane invaginations that could indicate scission

failure and defective endocytosis, although uptake of extracellular membrane appears to proceed in spite of the morphological aberrations^{16,17}. Deletion of Inp52 along with Rvs167 increases scission failure rate, supporting a possible role in membrane scission¹⁸. Loss of *inp51* mutation shows a increase in bulk PIP2 level, although changes in PIP2 levels have not been reported for mutations of *inp52*, and are not measured locally at the endocytic sites^{19,20}.

3.4.2.1 Synaptojanin-like Inp52 localizes to endocytic sites in the late scission stage

Of the three synaptojanin-like proteins in yeast, Inp51, Inp52, and Inp53, only Inp52-GFP localizes to cortical patches (Fig.3.6A) that co-localize with Abp1 (not shown). Inp51-GFP does not show any cortical patches: GFP-tagging either affects localization of the protein, or localization is too to be detected. Spatial and temporal alignment of Inp52-GFP to the endocytic timeline shows that it is localized to endocytic sites at the final scission stage, along with Rvs167. Spatial alignment with the coat protein Sla1 as reference shows that Inp52-GFP localizes to the tip of the membrane tube, and remains on the vesicle for a few seconds post scission: spatial and temporal localization of Inp52 is consistent with influence on scission, and could indicate a role for Inp52 in vesicle uncoating. Inp51-GFP does not show any cortical patches: GFP-tagging either affects localization of the protein, or localization is too to be detected. Rvs in single deletion strains show localizations similar to WT, but double deletion strains consists of large patches of Rvs167 at the plasma membrane, as well as localized within the cytoplasm.

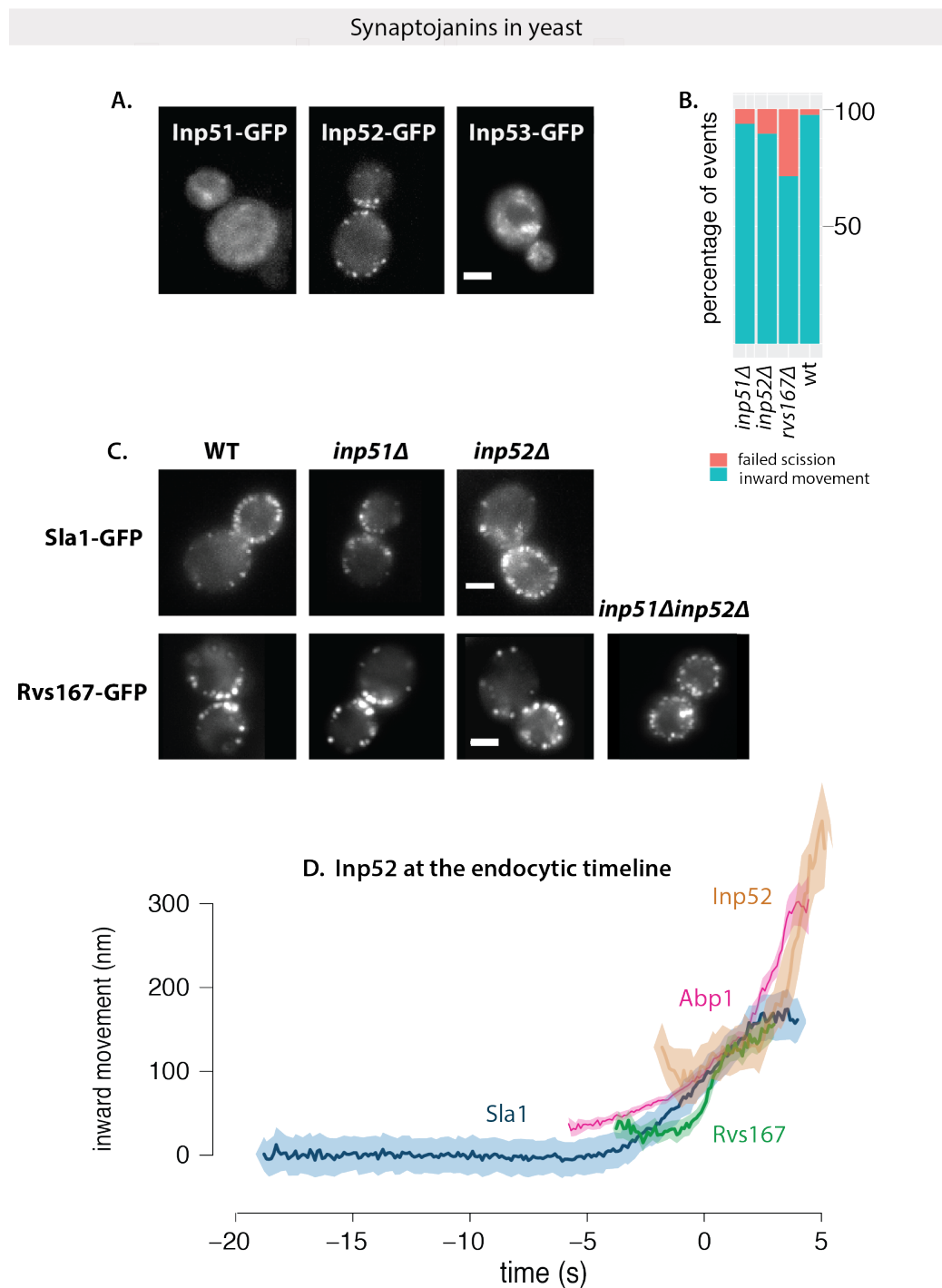


Figure 3.6: A: Maximum intensity projections of time-lapse images of cells expressing GFP-tagged Synaptojanin-like proteins Inp51, Inp52, and Inp53. Exposure rate 80ms. B: Failure rate of membrane scission, measured by quantifying number of retractions of Sla1 after membrane begins to move inwards, or by total lack of movement in WT, *rvs167Δ*, *inp51Δ* and *inp52Δ* strains. C: Sla1-GFP in WT, *inp51Δ* and *inp52Δ* strains show similar plasma membrane localization. Rvs167-GFP in WT, *inp51Δ*, *inp52Δ* and *inp51Δinp52Δ* strains. D: Inp52-GFP in endocytic timeline in WT cells. Time=0 (s) corresponds to scission time. All scale bars =2um.

3.4.2.2 Loss of yeast synaptojanins does not significantly affect coat and Rvs dynamics

In a model proposed by Liu et al, Synaptojanins and BAR proteins interact to regulate PI(4,5)P₂ hydrolysis, which in turn drives membrane scission. Here, the Rvs scaffold on the membrane tube protects the underlying PIP₂ from hydrolysis. Synaptojanin arrives at sites, and hydrolyses unprotected PIP₂. This generates a boundary between BAR-protected PIP₂ at the tube and PIP at the bud tip. The lipid boundary produces a line tension at the interphase that would generate enough force to pinch off a vesicle.

In order to test this model, I quantified coat and scission mechanics in *inp52Δ* cells. Deletion of Inp52 does not affect the speed of membrane invagination, or the maximum invagination length, as reported by the movement of the Sla1 centroid. Sla1-GFP patches are assembled and disassembled, as are Rvs167-GFP patches in *inp52Δ* cells (??). All-xxxxxx Sla1-GFP patches analysed (n=13 cells) move inwards. 72.9% of Rvs167-GFP patches move into the cytoplasm (n=4 cells, 37 patches). Remaining patches are disassembled without inward movement. Vesicle scission in *inp52Δ* occurs similar to WT, since the Rvs167 centroid moves inwards to approximately the same distance into the cytoplasm, indicating that the base of the vesicles are likely at the same position as in WT cells. Both Sla1 and Rvs167 centroids however, persist post-scission (arrowheads in figure) instead of disassembling immediately like in the WT. Since majority of the patches move inwards, and the increase in the lifetime of Rvs is post-scission, I find that the data is consistent with a role for Inp52 in vesicle uncoating, rather than a primary role in membrane scission, with the aberrations in plasma membrane morphology consequent of failure to recycle components, rather than scission.

I also quantified the coat and scission dynamics *inp51Δ*, since PiP₂ levels have been found to increase in *inp51Δ* cells. Loss of Inp51 does not affect Rvs167 or Sla1 centroid movement. All Sla1-GFP patches move inward (n=19 cells). 93% of Rvs167-GFP patches move inward (n=3 cells, 44 patches), similar to WT. Assembly of Rvs167 in the *inp51Δ* is slowed, the implication of this delay is not thus far clear.

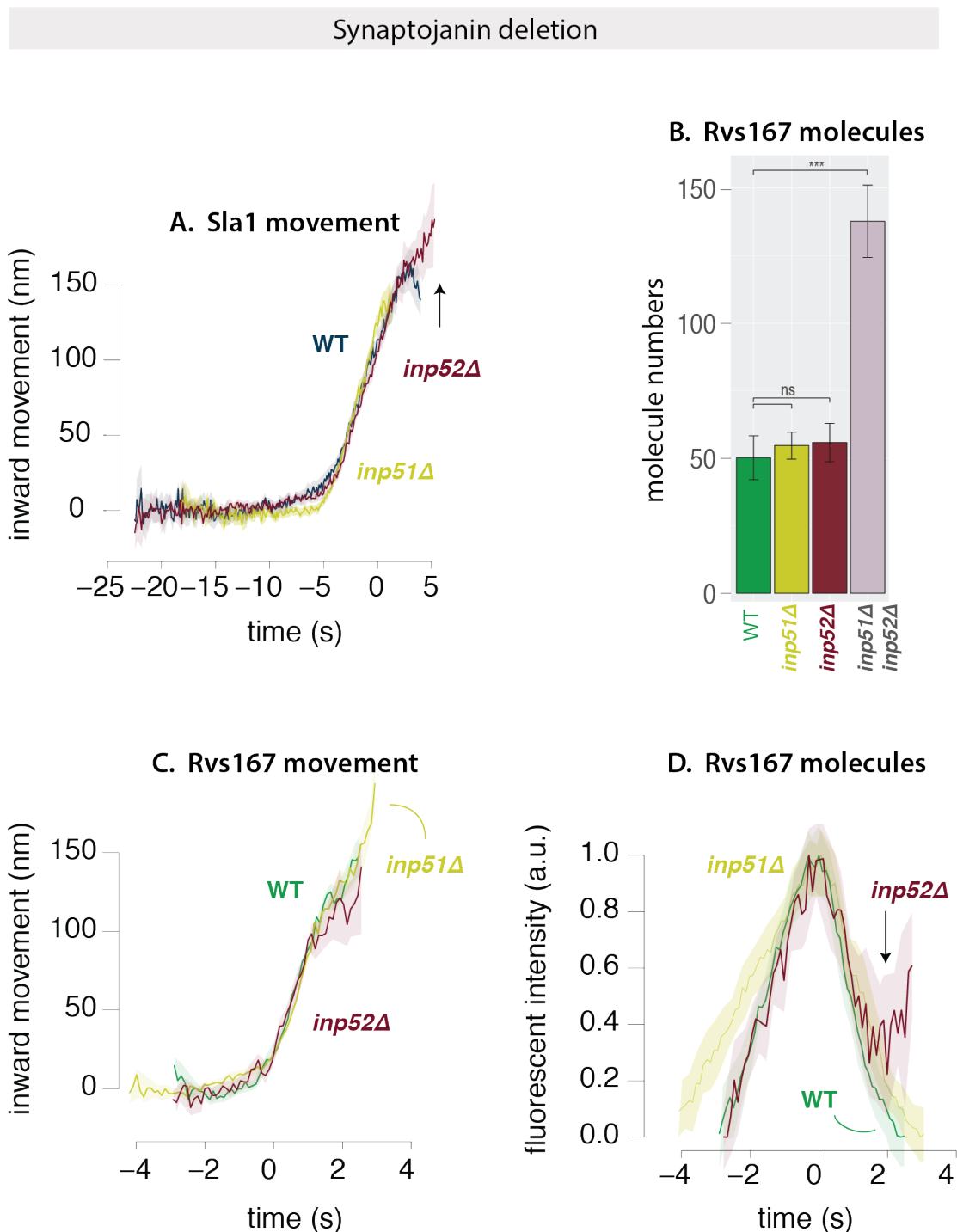


Figure 3.7: A: Movement of Sla1 in WT, *Inp51 Δ* and *Inp52 Δ* strains. B: Median number of Rvs167 molecules recruited to endocytic sites in WT, *inp52 Δ* , *inp52 Δ* and *inp51 Δ inp52 Δ* cells. P-values from two-sided z test, * = $p \leq 0.05$, ** = $p \leq 0.01$, *** = $p \leq 0.001$. C: Movement of Rvs167 in WT, *inp51 Δ* and *inp52 Δ* strains. D: Normalized fluorescent intensity of averaged Rvs167 patches in WT, *inp51 Δ* , *inp52 Δ* cells.

3.4.3 Membrane scission as a result of protein friction

Recent in-vitro experiments have proposed protein friction as a mechanism by which membrane scission could occur via BAR domain proteins in the absence of dynamin²⁴. In this model, a BAR domain scaffold on a membrane tube forms a frictional barrier to lipid diffusion. Forces that pull on the membrane, such as those exerted by motor proteins like myosins or actin polymerization, increase the frictional force exerted by the scaffold on the underlying membrane tube, increasing membrane tension in the bare region of the tube caused by membrane thinning from the lack of lipid influx to this region. Eventually, membrane pores form in this portion of the tube, leading to breaking the tube, and formation of a vesicle. Such a friction-dependent membrane scission model would predict that if more BAR proteins are added to the membrane, frictional force would increase, and scission should occur faster, that is, at shorter invagination lengths than with fewer BAR proteins. Essentially, this model requires a friction-inducing BAR scaffold, and a force that pulls the membrane under it. In yeast CME, this combination is provided by the Rvs complex and polymerization of the actin network respectively.

3.4.3.1 Membrane scission does not occur at shorter tube lengths when amount of Rvs is increased

To test whether protein friction could influence membrane scission in yeast, I duplicated the Rvs167 and Rvs161 genes as described in Huber et al.²¹. Gene duplication is performed in haploid cells to produce strains that have one (WT number) and two copies of both Rvs161 and Rvs167.

By quantifying the number of Rvs167 proteins as described in Picco et al., 12 in the haploid strains, I found that the average maximum number of Rvs molecules recruited to endocytic sites is increased, to 179.7328 +/- 10.1, from 113.505 +/- 5.2 in WT: 1.6x Rvs is recruited to endocytic sites in the duplicated strain. The averaged trajectory of Sla1-GFP, however does not change between the 4x and 2x copies of Rvs: like in the WT, Sla1 moves in to 140nm. The dynamics of Rvs, however is changed: In Fig.?? , the centroid movement of both Rvs167-GFP in WT and 2x RVS is aligned so that time=0 corresponds to the maxima of the fluorescent intensity, which corresponds to scission time. Molecule numbers of 2x Rvs increase at a faster rate than WT, and the disassembly is slowed by 1 second.

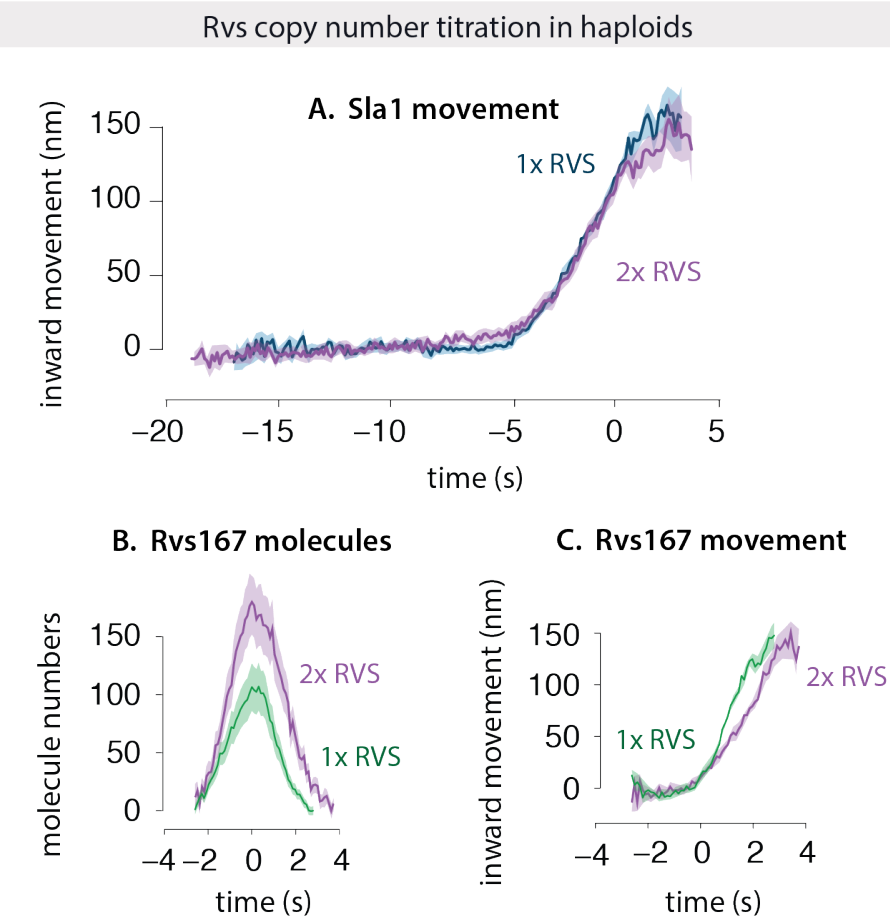


Figure 3.8: A. Movement of Sla1 in WT (1x RVS) and gene-duplicated Rvs (2x RVS) cells. 1x RVS Sla1 is aligned so that time=0 (s) is scission time. 2x RVS Sla1 is shifted to move inwards at the same time. B. Recruitment of Rvs167 to sites in WT (1x Rvs) and gene-duplicated Rvs (2x RVS) cells. 1x RVS is aligned so that time = 0 (s) is scission time. 2x RVS Sla1 is shifted to move inwards at the same time. C. Movement of Rvs167-GFP in WT (1x RVS) and gene-duplicated Rvs (2x RVS) cells. 1x RVS Rvs167 is aligned so that time=0 (s) is scission time. 2x RVS Rvs167 is shifted to move inwards at the same time.

In the corresponding Rvs movement trace, instead of the sharp jump seen in WT, there is a delay in the movement into the cytoplasm.

3.4.3.2 Scission timing occurs at a specific amount of Abp1, independent of the amount of Rvs recruited

The gene duplicated haploid strains are then crossed, so that diploid strains are generated that have 4x copies of the Rvs167 and Rvs161 genes, 2x copies each (WT number). Strains containing 1x copy of each Rvs is generated by crossing *rvs167* Δ strain with an *rvs161* Δ strain. I quantify Rvs recruitment, coat movement, and scission dynamics in these diploid strains, to study membrane scission as a function of Rvs copy number

In diploid cells, recruitment of Rvs is not directly proportionate to gene copy number: maximum number of Rvs recruited increases from $100.9 +/- 4.6$ in the 2x Rvs strain to $142.5, +/- 5.5$ in the 4x strain. In the 1x Rvs strain, $80.2, +/- 4.7$ molecules of Rvs are recruited before scission occurs. In order to determine whether this is a reflection on protein availability or if something else limits recruitment of Rvs, I quantified the cytoplasmic intensity of Rvs167-GFP in the respective strains by first producing z-stacks of time-lapse images of cells, and measuring the intensity within the cytoplasm (for details see METHODS). As can be seen in TABLE.X, the number of molecules recruited to endocytic sites scales with the amount of protein in the cytoplasm.

Inward movement of the Rvs centroid is similar for the 4x, 2x and 1x Rvs: the jump inwards is about 80nm. In the 1x strain, however, the centroid disappears immediately after scission, suggesting that there is reduced Rvs at the base of the newly formed vesicle compared to the WT. Recruitment dynamics of all three are different: in the 4x Rvs strain, Rvs is recruited at a rate of 57 molecules/second, which is reduced to 27 molec/sec for the 2x and 19.07 molec/sec for the 1x strain.

Sla1 centroid movement, meanwhile is the same in 4x and 2x Rvs strains. In the 1x Rvs strain, Sla1 movement is slightly decreased, suggesting that vesicle scission occurs at invagination lengths about 10nm shorter than that as WT when fewer Rvs molecules are recruited, but increasing Rvs recruitment does not affect membrane progression.

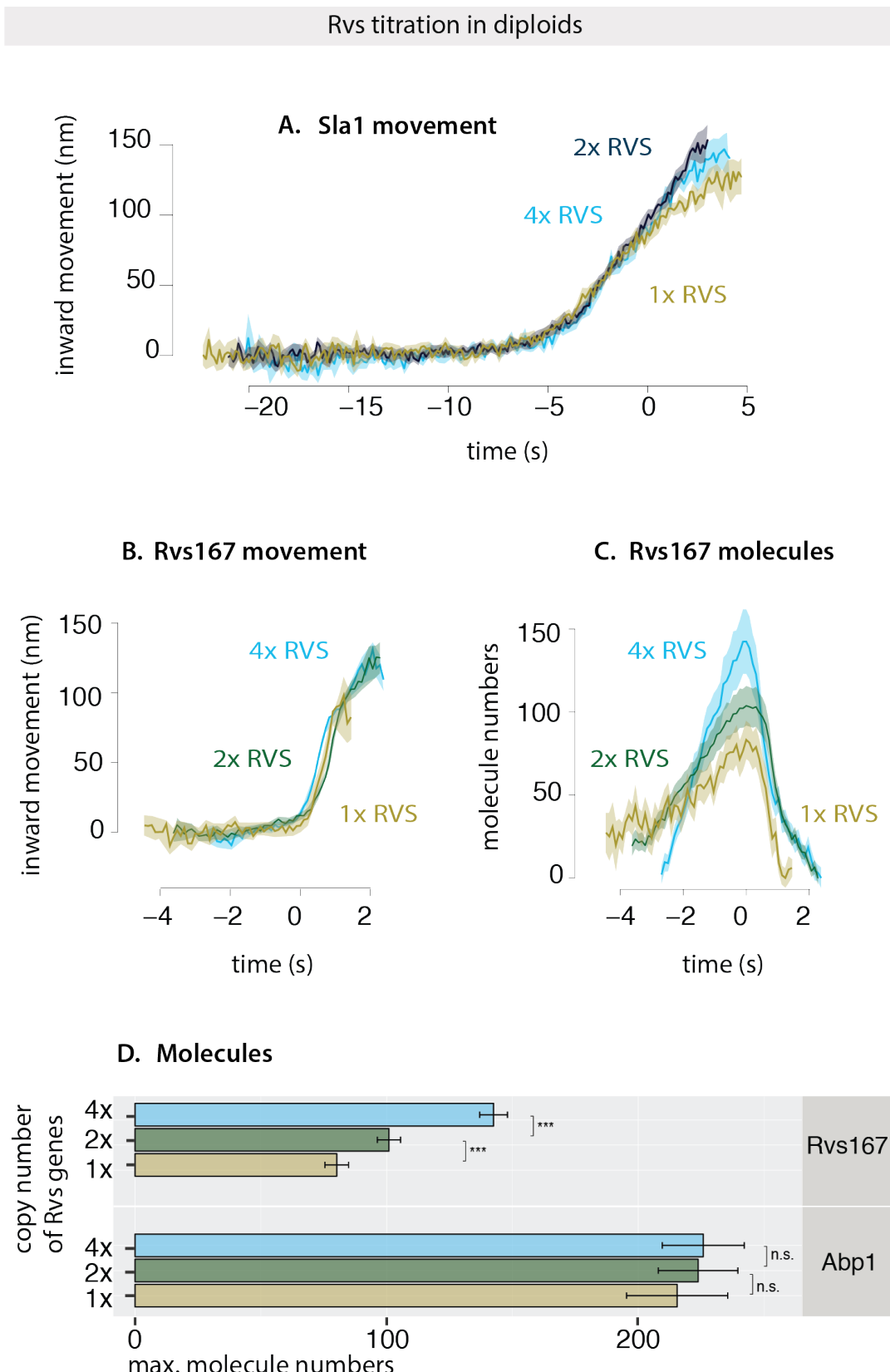


Figure 3.9: A. Movement of Sla1 in WT (1x RVS) and gene-duplicated Rvs (2x RVS) cells. 1x RVS Sla1 is aligned so that time=0 (s) is scission time. 2x RVS Sla1 is shifted to move inwards at the same time. B. Recruitment of Rvs167 to sites in WT (1x Rvs) and gene-duplicated Rvs (2x RVS) cells. 1x RVS is aligned so that time = 0 (s) is scission time. 2x RVS Sla1 is shifted to move inwards at the same time. C. Movement of Rvs167-GFP in WT (1x RVS) and gene-duplicated Rvs (2x RVS) cells. 1x RVS Rvs167 is aligned so that time=0 (s) is scission time. 2x RVS Rvs167 is shifted to move inwards at the same time.

3.4.4 BAR domains as membrane scaffolds

3.4.4.1 Localization of BAR domain alone prevents membrane scission

In haploid cells, Rvs167 expressed without the SH3 domain is recruited in lower numbers than the full-length protein (Fig.1B right), although cellular expression of the protein is the same as the WT (not shown). Sla1 movement in *rvs167ΔSH3* cells is reduced to close to *rvs167Δ* lengths (Fig.4 left). When the Rvs167 gene is duplicated without the SH3 domain, the number of *rvs167ΔSH3* molecules recruited to endocytic sites are increased, and correspondingly, Sla1 movement increases from the *rvs167Δ* lengths towards the WT lengths (Fig.4): shallow invaginations of the *rvs167Δ* can be rescued by recruiting only BAR domains of Rvs167.

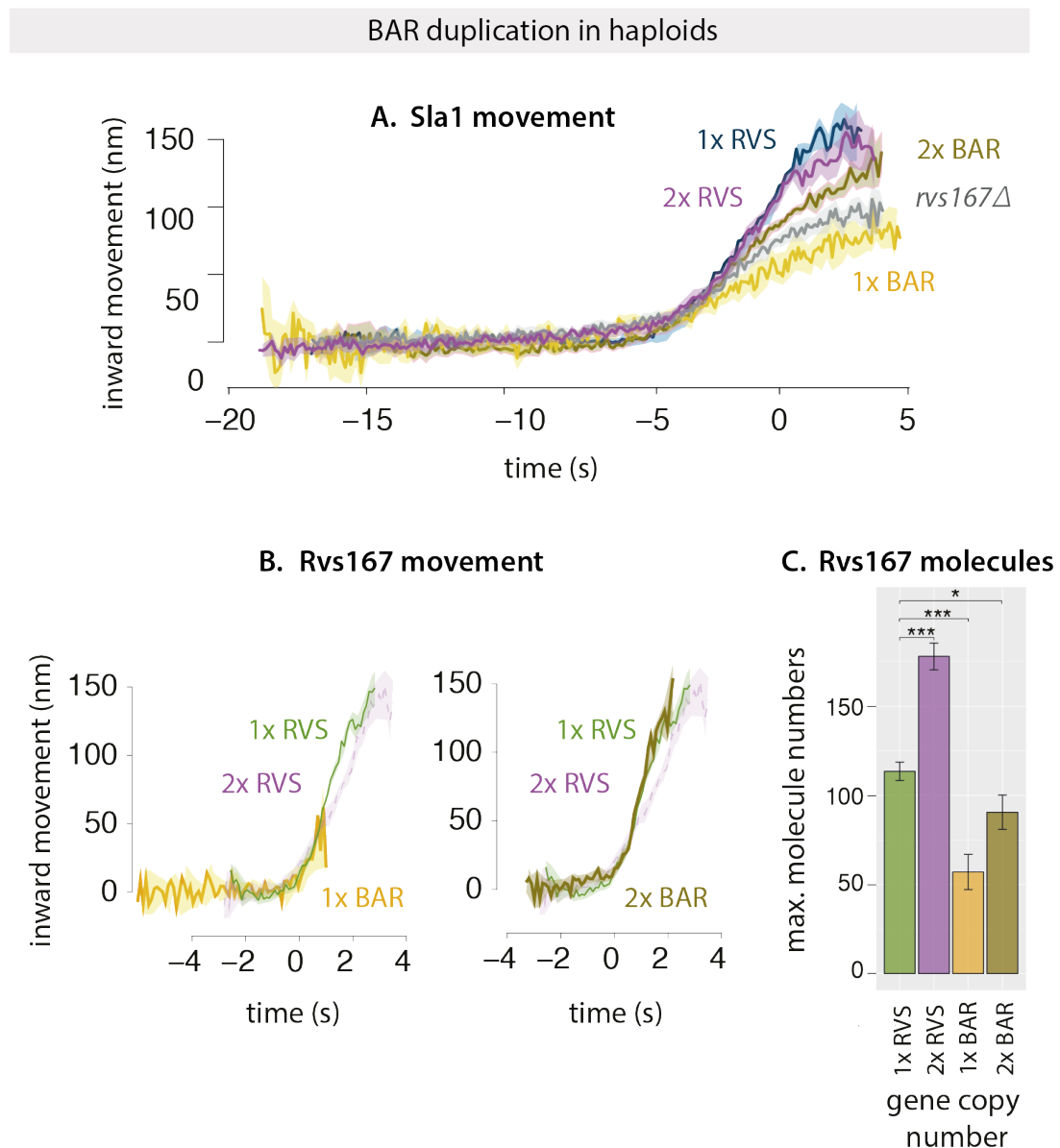
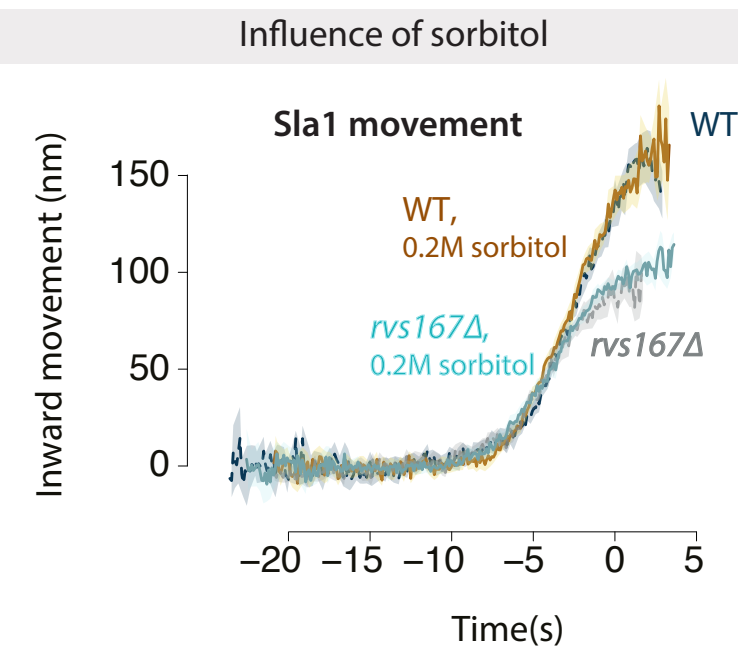


Figure 3.10: A: Averaged centroid movement of Sla1 in strains expressing varying gene copy numbers of Rvs complex, and *rvs167* Δ . 1x Rvs=WT expression, 2x = Rvs167 and Rvs161 genes are duplicated. 1xBAR=Rvs167 without the SH3 domain, 2xBAR=Rvs167 without the SH3 domain is duplicated. Averages are aligned in time so that time=0 (s) for WT Sla1-GFP corresponds to scission time. Other averages have been shifted to move inwards at the same time as the WT. B: Averaged centroid movement of Rvs167-GFP in 1x RVS, 2xRVS, 1xBAR, 2XBAR strains. C:

3.4.5 Membrane dynamics with reduced membrane tension

Yeast cells are under high turgor pressure by virtue of the rigid cell wall, expected to be several orders of magnitude higher than cultured mammalian cells. Forces from actin polymerization are hence necessary to overcome this resistance to membrane bending. Membrane tension, which also contributes to the resistance to bending, has a large influence on the forces required to invaginate the membrane. Osmotic pressure, and therefore, membrane tension can be controlled



4 | Discussion

The recruitment and function of the Rvs complex in the last scission stage of endocytosis has been explored in this work, as well as some previously untested proposals for how membrane scission could be effected in yeast endocytosis. I propose that Rvs localizes by interactions of the BAR domains of the Rvs complex with invaginated membranes, and that the SH3 domain is required for efficient and timely recruitment of Rvs to sites. Arrival of Rvs on membrane tubes then scaffolds the membrane tube and prevents membrane scission, in a manner that depends on recruitment of a critical number of Rvs molecules, till actin forces rupture the membrane, causing vesicle scission.

Here I discuss the main findings of this thesis in support of these propositions.

4.1 Recruitment of Rvs to endocytic sites

Rvs is relatively short-lived protein at endocytic sites, recruited in the last stage, to membrane tubes^{1–3}: timing and position appear to be tightly regulated. FCS measurements have shown that the cytoplasmic content of Rvs¹⁶⁷, as well as that of Rvs¹⁶¹ is quite high compared to other endocytic proteins⁴: many early proteins, and several of the later WASP/ Myosin module like Las¹⁷, Vrp¹, type¹ myosins, are measured at 80–240nM, while cytoplasmic intensity of 161 is 721nM, and 167 is measured at 354nM. In spite of this, relatively few numbers of Rvs are recruited to endocytic sites, suggesting that cytoplasmic concentration alone does not determine recruitment dynamics. Comparison between FCS measurements of cytoplasmic concentration for different endocytic proteins, and their recruitment to the endocytic sites indicates low correlation between the two, perhaps unsurprisingly, requiring that other directed mechanisms recruit proteins in a timed and efficient manner. In the case of Rvs, both

timing and efficiency appear crucial to its function, the question is what confers both.

4.1.1 Timing of localization and efficiency of recruitment

4.1.1.1 The BAR domain senses membrane curvature

Rvs167 recruitment has been correlated against membrane shapes along the endocytic timeline. CLEM studies have shown that when Rvs arrival is plotted against the smallest angle between the two membrane sides², which is 180 when the membrane is flat, and goes to 0 as the membrane becomes tubular, at the time of the recruitment of Rvs, this angle is 0. This indicates that Rvs is recruited only to tubular membrane shapes. From the curved structure of the BAR dimer, it has been assumed that it is recruited by its preference for some membrane shapes over others. In the absence of membrane curvature, in *sla2del* cells, the Rvs BAR domain does not localize to cortical patches. This demonstrates for the first time that this BAR domain does indeed sense and requires membrane curvature to localize to cortical patches. BAR recruitment by sensing membrane curvature would allow for this specificity. Work on BAR domains have so far not uncovered a specific interaction with a lipid subtype, and have suggested that hydrophobic interactions mediate this interaction. It is not clear how the Rvs BAR domains interacts with the membrane, and mutations of the lipid-binding surfaces are necessary to clarify the interaction with underlying lipids.

4.1.1.2 BAR domain times recruitment of Rvs

Without the SH3 domain, that is in BAR cells, Rvs167 is able to localize to endocytic sites, and has a similar lifetime. In Fig3.4 A, B, Abp1 and Rvs167 in WT and BAR cells are aligned in time to the peak of the respective Abp1 fluorescent intensities. There are two striking differences when comparing the timing of proteins in the two cases: first, while WT Rvs arrives about 4 seconds after the arrival of Abp1, Rvs in BAR cells arrives only 6 seconds after Abp1 arrives. There is a time delay between Abp1 arrival and Rvs167 recruitment in BAR cells, confirmed by the TIRF measurement in 3.4D. The timing of Rvs arrival could be determined either by BAR interaction with membrane curvature, or by an SH3 interaction with an unknown binding partner. Rvs in BAR cells arrives when Sla1 has moved inwards 25-35nm, which is also the Sla1 distance moved when Rvs in WT arrives. This means

that Rvs recruitment is delayed in BAR cells, since Sla1 moves inwards slower, and until an invagination of a specific length is formed. This suggests that what times Rvs recruitment to endocytic sites is a particular membrane invagination length, and that this timing is provided by the BAR domain interaction. To be noted is that Sla1 is not directly at the plasma membrane, and the centroid of Sla1 sits about 20nm higher on the flat plasma membrane than Sla2. Therefore, a 25-35 distance of Sla1 would correspond to 45-55 nm of membrane invagination, by which point, the membrane is already parallel, and this is consistent with Rvs arrival at invaginated tubes.

4.1.1.3 SH3 domain regulates actin network

Another observation is that Abp1 accumulation is aberrant in BAR cells: it accumulates at the same rate as in WT cells till a point, and then slows dramatically, and stops at about half the WT Abp1 numbers. The point the accumulation slows is interesting: it is at the time at which Rvs in WT cells arrives at endocytic sites. This could mean that SH3 domains are involved also in regulation of the actin network. Disassembly of Abp1 begins at the same time in BAR and WT cells, at shorter invagination lengths, and at lower Abp1 levels. This could indicate that Abp1 disassembly is triggered by an external "timer" (marked by the dashed red line in Fig.3.4B).

While in the WT cells, peaks of Abp1 and Rvs167 fluorescent intensity and consequent decay coincide, this is not true for the BAR cells. Rvs in these cells peaks several seconds after Abp1 intensity starts to drop. Abp1 drop indicates the disassembly of the actin network after vesicle scission. In WT cells, this drop coincides with a fast inward movement of the Abp1 centroid into the cytoplasm, and concomitant Rvs drop indicates membrane scission. A decoupling of the two could indicate that the actin disassembly and membrane scission do not coincide in BAR cells. The source of the Abp1 and Rvs167 peak mismatch in BAR cells is unclear. Since Rvs molecules in BAR cells sense membrane curvature, it is mostly likely that the BAR dimers are interacting with the membrane tube, so the decay in Rvs intensity in BAR cells most likely indicates membrane scission, also supporting the idea of an external timer for the disassembly of Abp1, and perhaps the entire actin network. This could imply that Abp1 is disassembled from the actin network before membrane scission.

Abp1 is an activator of the Arp2/3 complex

4.1.1.4 The SH3 domain makes Rvs localization efficient

Cellular expression alone does not determine how much Rvs gets recruited: as has been shown in Results 3.3, Rvs in BAR cells accumulates to about half its wild-type number, even though the same cytosolic concentration is measured (see methods). This indicates that the SH3 domain increases the efficiency of recruitment of Rvs to invaginated tubes. The decreased number of Rvs molecules recruited reduces the inward movement of Sla1 to similar to rvs167del cells, is discussed in the later section.

4.1.1.5 The SH3 domain can assemble and disassemble Rvs molecules

Transient cortical patches in LatA treated cells expressing Rvs167-GFP that are absent in LatA cells expressing rvs167Δ SH3-GFP (Fig.1A) suggests that the former patches are caused by an interaction mediated by the SH3 domain. These patches suggest that the SH3 domain is able to cluster protein to the cell cortex, although the mechanism by which this occurs is not known.

Full-length Rvs is able to localize to cortical patches without the membrane-dependent interaction of the BAR domain (Fig. Full-length RVS in sla2del and LatA treatment shows cortical patches). This indicates that the SH3 domain is able to mediate recruitment of a cluster of Rvs molecules, and then disassemble this cluster. The independent ability of the SH3 domain to localize and disassembly protein complexes is surprising, since SH3 domains are known so far to mediate protein-protein interaction and self-regulation of activation states.

What does the SH3 domain interact with? SH3 interaction with an endocytic binding partner could help recruit Rvs to sites. Many such interaction partners have been proposed; Abp1 interaction with the Rvs167 SH3 domain has been shown^{5,6}, Las17^{7,8}, Cmd19, type I myosins¹⁰, Vrp15, which recruits the myosins, have all emerged as potential candidates, and are being studied as potential targets of the Rvs167 SH3 domain. Since the SH3 is able to localize to endocytic sites in an actin independent manner, the interaction candidate is likely one that does not require actin, leaving Vrp1, Las17, type1 myosins Myo3/5. Las17 and type 1 myosins localize to the base of the invagination, and do not move into the cytoplasm a significant amount during invagination. If one of these was the SH3 interaction partner, SH3 domains are then recruited at the base of

the invagination, and then pushed up with membrane as the tube grows longer. Centroid tracking however, suggests that Rvs is accumulated all over the membrane tube without bias towards the base of the invagination: if this was the case, the centroid would move upwards rather than remain non-motile. It is possible for the SH3 to drive early recruitment and localization, which is then "switched off" as Rvs is clustered by the SH3 domain, and targeted recruitment via an interaction partner is no longer necessary.

4.1.2 Arrangement of Rvs

It is unclear how Rvs is arranged on the membrane tube. Although solved structures of BAR domains show high structural similarity in spite of low sequence similarity, no structure for the Rvs complex exists. The fact that this is a hetero- rather than homodimer suggests that the structure does not necessarily resemble that of Amphiphysin or Endophilin homodimers, and a high-resolution structure will be necessary to clarify the interaction and arrangement of Rvs on endocytic tubes

4.1.2.1 Rvs does not form a tight scaffold on yeast membrane tubes

Cryo EM structures of mammalian BAR proteins have suggested that the BAR dimers of Rvs might form a similar helical scaffold with lateral interactions between adjacent BAR domains on invaginated membrane tubes. In the Rvs overexpression strains in diploids, Rvs can be recruited in much higher numbers, and at a much faster rate to the membrane than in WT cells, but appears to have similar disassembly dynamics as in the WT (Fig.5). The atypical, sharp decay fluorescent signal indicates that all of the Rvs on the membrane is suddenly released, consistent with the idea of a scaffold that breaks upon vesicle scission, releasing all the membrane-bound BAR protein. The decay in the 4x Rvs strain suggests that all the Rvs is also bound to the membrane, and since the membrane is now able to accommodate about 1.6x the amount of BAR protein as the WT on the same amount of membrane, it appears that in the WT case, a tight helix that covers the entire tube was not likely to be formed: adding molecules to such a tube would result in a change in at least disassembly dynamics.

4.1.2.2 A limit for how much Rvs can be recruited to the membrane

A change in disassembly dynamics is seen, however, in Rvs duplication in haploid cells. In this case, an even higher amount of Rvs is recruited to cells than in the WT: the maximum number of molecules recruited before scission is $178 +/- 7.5$ compared to $113.505 +/- 5.2$ yields a $1.57\times$ recruitment of protein to membrane tubes. Here, the disassembly of Rvs after scission is delayed, and would suggest that the excess protein is not directly on the membrane. The excess Rvs either interacts with the actin network via the SH3 domain, or interacts with other Rvs dimers. Currently, I am not able to distinguish between the two, since the SH3 interaction partner is currently undetermined, and the arrangement of Rvs on the membrane is currently unknown. BAR-BAR interactions have been observed for other BAR proteins, albeit via lateral interactions at the tips of the curved structure, between apposed BAR domain. The concave face of BAR domains has been shown to interact with the membrane, and interactions that allow concentric arrangement of BAR domains are not seen before and are unlikely, but perhaps still possible.

Whatever the arrangement of the Rvs complex on the membrane, that the disassembly dynamics is changed in the case of $1.6\times$ Rvs, compared to WT, and $1.4\times$ Rvs suggests that there is a limit to how much Rvs can assemble on the tube without a change in protein-protein or protein-membrane interaction. Why there is a difference between recruitment of Rvs in the diploid and haploid case is uncertain. Diploid cells do not double in volume compared to haploids: in normal growth conditions, the volume of the diploid cell varies between $1.57\times$ that of the haploid cell, and the average cell surface area increases by 1.4×11 . In the gene duplication case, we have two copies of Rvs that in principle should be expressed at twice the haploid level. Cytoplasmic quantification, however, shows that the increase is $1.4\times$ in the duplicated diploid case compared to the WT diploid case, as does the recruitment to endocytic sites. There is then $1.4\times$ the protein in nearly $1.6\times$ the cellular volume, resulting in a dilution of the protein content per unit volume of the cell, which could then explain the decreased recruitment.

It appears that the recruitment is then proportionate to gene copy number, and protein content in the cell, but that this is not the only factor that influences recruitment.

4.1.3 Rvs161 and Rvs167 are recruited as dimers to endocytic sites

FCCS and genetic studies have both proposed that the Rvs complex is recruited to endocytic sites as heterodimers, although the deletions of one do not exactly match the deletion of the other. Deletion of Rvs161, for example, confers a defect in cell fusion, that is not present in the rvs167 deletion. FCCS measurements have indicated that Rvs167 and Rvs161 form stable heterodimers in the cytoplasm, although they appear to be expressed at different concentration. Cytoplasmic concentration of 161 is expressed at 721nM by FCS, while 167 is measured at 354nM, suggesting a nearly two-fold increase in expression of 161. Overexpression of 167 in the duplicated strain, however, does not lead to increased recruitment of that protein to endocytic sites, unless matched by overexpression of Rvs161. In the case of overexpression of BAR, without overexpression of 161, however, there is an increased recruitment of BAR to sites. Cytoplasmic background quantification has shown only a moderate decrease in the expression of BAR, compared to full-length Rvs167. This leads to a conundrum of recruitment: how does more BAR lead to more protein, while more 167 does not? I propose that

4.1.3.1 Contribution of the N-amphiphatic helix and GPA region

The influence of the N-terminal amphiphatic helix (N-helix) and the unstructured GPA region have not been studied in this work. Preliminary results (not shown) indicate that removal of the N-helix does not prevent recruitment of endocytic sites. Other work has shown that N-helix is not necessary for localization of the protein, except in high salt conditions, and could aid clustering of the protein at endocytic sites in normal growth conditions. The GPA region is thought to function as the linker between the BAR and SH3 regions, and no other specific function is known.

4.2 What causes membrane scission?

4.2.1 Dynamin does not drive scission

Some studies have suggested that Vps1 does localize to endocytic sites, and affects the scission mechanism: Nannapaneni et al.,²³ find that the lifetime of Las17, Sla1, Abp1 increase in the absence of Vps1. Rooij et al.,²⁴ find that Rvs167 lifetimes increase, and are recruited in fewer patches to

the cell cortex. On the other hand, *vps1Δ* did not increase the scission failure rate of *rvs167Δ* in other studies²⁵, and did not colocalize with other endocytic proteins²⁶. We see a slight but insignificant increase in Rvs167 lifetimes in *vps1Δ* cells. If Vps1 was to affect scission, the number of failed scission events should increase in *vps1Δ* cells, and increase the lengths of invaginated tubes, but we do not find so. The lack of influence of Vps1 on coat and scission dynamics shows that membrane scission is not dependent on a dynamin interaction. Vp1 tagged with super-folded GFP and imaged in TIRF does not form cortical patches that co-localize with Abp1-mCherry (data from Andrea Picco, not shown). That tagging does not cause the slight growth defect of the *vps1Δ* cells is seen in dot spot assays. GFP-tagging could however, affect the recruitment of Vps1 to endocytic sites while maintaining its role in other cellular processes like vesicular trafficking. Outside of potential issues recruiting the protein to endocytic sites, membrane movement and scission dynamics are unchanged in the absence of Vps1, suggesting that even if it recruited to sites, it is not necessary for Rvs localization or function.

4.2.2 Lipid hydrolysis is not the primary cause of membrane scission

Inp51 is not seen to localize to the cellular cortex, but cytoplasmic concentration measured by FCS is low, suggesting low levels of expression that are likely undetected by our imaging protocol. Inp52 localizes to the top of invaginations right before scission, consistent with a role in vesicle formation.

However, the synaptojanin-mediated scission model¹⁹ predicts that first, vesicle scission would occur at the top of the invaginated tube, at the interphase of the hydrolyzed and non-hydrolyzed lipid. Kukulski et al.,¹⁶ have shown that vesicles undergo scission at 2/3 the invagination depths: that is, vesicles generated by lipid hydrolysis based line tension would be smaller than have been seen. Second, removing forces generated by lipid hydrolysis by deleting synaptojanins should then increase the invagination lengths measured. Deletion of Inp51 and Inp52 do not change the invagination depths at which scission occurs, as measured from the maximum movement of Sla1. That the position of the vesicle formed is also unchanged is indicated by the magnitude of the jump into the cytoplasm of the Rvs complex.

There are some changes, however in the synaptosomal deletion strains. First, in the *inp51del* strain, Rvs assembly is slightly slower than that of the WT. Thus far, it is unclear what this means. Rvs centroid persists after scission for about a second longer than the WT does, indicating that disassembly of Rvs on the base of the newly formed vesicle is delayed. In the *inp52del* strain, about 12% of Sla1-GFP tracks do not move into the cytoplasm and undergo scission. Although this is low compared to the failed scission rate of the *rvs167del* cells (close to 30%), it could suggest a moderate influence of *inp52* on scission dynamics. In the *inp5152del* strain, Rvs is accumulated at patches, but most Rvs patches do not show the sharp jump into the cytoplasm. Membrane morphology is hugely aberrant in these cells, complicating the interpretation of this data. Electron microscopy shows long, undulating membrane invaginations, with multiple endocytic sites that are assembled and disassembled. Where the Rvs complex localizes in these cells could be clarified by CLEM or superresolution microscopy. Large clusters of Rvs on the same invaginated tube would influence the molecule numbers acquired by this kind of analysis, and yield a higher number than at a single site (although what is actually happening at these patches is not actually clear). Rvs does, interestingly, assemble and disassemble. If there is no vesicle at these membrane, it would indicate that Rvs disassembly is decoupled from membrane scission.

4.2.3 Protein friction does not drive membrane scission

In Rvs duplicated strains, adding up to 1.6x the WT amount of Rvs to membrane tubes does not affect the length at which the membrane undergoes scission. The protein friction model introduced in Section 4.2.3 would suggest that if more BAR domains were added to the membrane tube, the frictional force generated as the membrane is pulled under it would increase, and the membrane would rupture "faster", that is, as soon as WT forces are generated on the tube. In the haploid duplication strain, the WT amount of Rvs is recruited at nearly -2 seconds, but scission does not occur at this time point. In the diploid strains, meanwhile, adding 1.4x the WT amount of Rvs does not change length of membrane scission. Decreasing the amount of Rvs from WT amounts, like in the 1x Rvs strain, however reduces the scission efficiency, and slightly reduces the inward movement of the membrane.

4.2.4 Actin polymerization generates forces required for membrane scission

4.3 Function of the Rvs complex

4.3.1 Rvs scaffolds membrane pore

From the *rvs167Δ* coat movement, it looks like Rvs is required to prevent membrane scission. This could be effected by either a BAR-interaction that would support the membrane tube, and prevent membrane scission, or an SH3 dependent mechanism that would perhaps modulate actin dynamics, and prevent forces from being transmitted efficiently to the membrane neck, and prevent scission. From the BAR duplication experiments, longer invaginations that the *rvs167Δ* or the BAR can be reconstituted by simply adding more BAR domains. This supports the idea that preventing membrane scission by preventing fusion of the inner lipid bilayer in the membrane tube is the mechanism of action.

4.3.2 A critical amount of Rvs is required to allow invaginations to grow

Sla1 in *rvs167Δ* cells undergoes scission at short invagination lengths of about 60nm (Fig.4), compared to the WT lengths of 140nm¹⁶; Rvs167 is required at membrane tubes to prevent premature scission. In BAR cells, half the WT amount of Rvs is recruited, and coat dynamics resemble that of *rvs167Δ*. This indicates that a threshold amount of Rvs is required to recapitulate WT endocytic dynamics.

This is consistent with the SH3 domain mediating actin forces to the invagination neck, causing scission, as well as with Rvs167 stabilizing the membrane invagination via membrane interactions of the BAR domain³³. Since WT invagination depths are reproduced by overexpression of the BAR domain alone, we propose that localization of Rvs to the membrane tube stabilizes the membrane pore, and allows deep invaginations to grow until actin polymerization produces enough forces to sever the membrane and cause scission. Here, the forces are generated entirely by actin polymerization, and the amount of force necessary is determined by the physical properties of the membrane.

4.4 Role of other scission-stage proteins

4.4.1 Inp52 is likely involved in uncoating vesicles after scission

Deletion of Synaptojanin-like Inp52 does not affect the invagination depths of Sla1, but Sla1 patches persist for longer after scission in the *inp52Δ* than in WT cells, as do patches of Rvs167, indicated by the arrows in Fig.2. Both delays suggest that rather than the scission time-point, post- scission disassembly of proteins from the vesicle is inhibited by the deletion, and that Inp52 plays a role in recycling endocytic proteins to the plasma membrane.

4.5 Model for membrane scission

4.6 Other potential scission mechanisms and open questions

does the Nhelix influence anything? why these curvatures? specificity from the SH3 domain? why does it come off

5 | Materials and Methods

5.1 Materials

5.1.1 Yeast strains

STRAIN	GENOTYPE
MKY0100	MAT α , his3 Δ 200, leu2-3,112, ura3-52, lys2-801
MKY0102	MAT α , his3 Δ 200, leu2-3,112, ura3-52, lys2-801
	MAT α /MAT α , his3 Δ 200/his3 Δ 200, leu2-3,112/leu2-3,112, ura3-52/ura3-52,
MKY0105	lys2-801/lys2-801
MKY0122	MAT α , his3 Δ 200, leu2-3,112, ura3-52, lys2-801, ABP1-EGFP::HIS3MX6
MKY0123	MAT α , his3 Δ 200, leu2-3,112, ura3-52, lys2-801, ABP1-EGFP::HIS3MX6
MKY0216	MAT α his3 Δ 200, leu2-3,112 ura3-52, lys2-801 NUF2-EGFP::HIS3MX6
MKY0217	MAT α his3 Δ 200, leu2-3,112 ura3-52, lys2-801 NUF2-EGFP::HIS3MX6
MKY0224	MAT α , his3 Δ 200 leu2-3,112, ura3-52, lys2-801 NUF2-mCherry::KANMX4
MKY0225	MAT α his3 Δ 200, leu2-3,112 ura3-52, lys2-801 NUF2-mCherry::KANMX4
	MAT α , his3 Δ 200, leu2-3,112, ura3-52, lys2-801,SLA1-EGFP::HISMX, ABP1-
MKY0822	mCherry::kanMX
	MAT α , his3 Δ 200, leu2-3,112, ura3-52, SLA1-EGFP::HISMX, ABP1-
MKY0823	mCherry::kanMX
MKY0141	MAT α , his3 Δ 200, leu2-3,112, ura3-52, lys2-801, SLA1-EGFP::HIS3MX6
MKY2832	Mat a, his3 Δ 200, leu2-3,112, ura3-52, lys2-801, Rvs167-EGFP::HIS3MX6
	MAT α , his3 Δ 200, leu2-3,112, ura3-52, lys2-801, Abp1-mCherry::KANMX4,
MKY3131	Rvs167-EGFP::HISMX6
	MAT α , his3 Δ 200, leu2-3,112, ura3-52, lys2-801, Abp1-mCherry::KANMX4,
MKY3132	Rvs167-EGFP::HISMX6
	Mat a, his3 Δ 200, leu2-3,112, ura3-52, lys2-801, rvs167- Δ SH3-
MKY3154	EGFP::HIS3MX6
	MAT α , his3 Δ 200, leu2-3,112, ura3-52, lys2-801, rvs167- Δ SH3::natNT2, ABP1-
MKY3201	EGFP::HIS3MX6

	Mat a/α, his3Δ200/his3Δ200, leu2-3,112/leu2-3,112, ura3-52/ura3-52, lys2-
MKY3258	801/lys2-801,Vps1-EGFP::HIS3MX6/Vps1, Abp1-mCherry::KANMX/Abp1
MKY3260	Mat a, his3Δ200, leu2-3,112, ura3-52, lys2-801, Vps1-sfGFP::URA3
	MAT α , his3Δ200, leu2-3,112, ura3-52, lys2-801, sla2::natNT2, rvs167-ΔSH3-
MKY3280	EGFP::HIS3MX6, SLA1-mcherry::kanMX5
	MAT α , his3Δ200, leu2-3,112, ura3-52, lys2-801, sla2::natNT2, rvs167-ΔSH3-
MKY3281	EGFP::HIS3MX6, SLA1-mcherry::kanMX5
	MAT α , his3Δ200, leu2-3,112, ura3-52, lys2-801, sla2::natNT2, RVS167-
MKY3282	EGFP::HIS3MX6, ABP1-mcherry::kanMX5
	MAT α , his3Δ200, leu2-3,112, ura3-52, lys2-801, sla2::natNT2, RVS167-
MKY3283	EGFP::HIS3MX6, ABP1-mcherry::kanMX5
	MAT α , his3Δ200, leu2-3,112, ura3-52, lys2-801, sla2::natNT2, rvs167-ΔSH3-
MKY3284	EGFP::HIS3MX6, ABP1-mcherry::kanMX5
	MAT α , his3Δ200, leu2-3,112, ura3-52, lys2-801, sla2::natNT2, rvs167-ΔSH3-
MKY3285	EGFP::HIS3MX6, ABP1-mcherry::kanMX5
	MAT α , his3Δ200, leu2-3,112, ura3-52, lys2-801, rvs167-ΔSH3-
MKY3286	EGFP::HIS3MX6, ABP1-mCherry::KANMX4
MKY3287	MAT α , his3Δ200, leu2-3,112, ura3-52, lys2-801 rvs167-ΔSH3::natN2
MKY3288	MAT α , his3Δ200, leu2-3,112, ura3-52, lys2-801, rvs167-ΔSH3::natNT2
	MAT α , his3Δ200, leu2-3,112, ura3-52, lys2-801, rvs167-ΔSH3::natNT2, SLA1-
MKY3289	EGFP::HIS3MX6
	MAT α , his3Δ200, leu2-3,112, ura3-52, lys2-801, rvs167-ΔSH3::natNT2, SLA1-
MKY3290	EGFP::HIS3MX6
	MAT α , his3Δ200, leu2-3,112, ura3-52, lys2-801, rvs167-ΔSH3::natNT2, ABP1-
MKY3291	EGFP::HIS3MX6
	MAT α , his3Δ200, leu2-3,112, ura3-52, lys2-801, rvs167-ΔSH3::natNT2, SLA1-
MKY3292	EGFP::HIS3MX, ABP1-mcherry::kanMX4
	Mat α his3Δ200, leu2-3,112, ura3-52, lys2-801, SLA1-mCherry::KANMX4,
MKY3295	sla2::NAT, RVS167-EGFP::HIS3MX6
MKY3339	MAT α , his3Δ200, leu2-3,112, ura3-52, lys2-801 vps1::natNT2
	MAT α , his3Δ200, leu2-3,112, ura3-52, lys2-801, vps1::natNT2, RVS167-
MKY3341	EGFP::HIS3MX6
	MAT α , his3Δ200, leu2-3,112, ura3-52, lys2-801, vps1::natNT2, RVS167-
MKY3342	EGFP::HIS3MX6
	MAT α , his3Δ200, leu2-3,112, ura3-52, lys2-801, vps1::natNT2, RVS167-
MKY3343	EGFP::HIS3MX6 , ABP1-mCherry::kanMX4
	MAT α , his3Δ200, leu2-3,112, ura3-52, lys2-801, vps1::natNT2, RVS167-
MKY3344	EGFP::HIS3MX6 , ABP1-mCherry::kanMX4

	MAT α , his3 Δ 200, leu2-3,112, ura3-52, lys2-801, vps1 Δ ::natNT2, SLA1-
MKY3345	EGFP::HIS3MX6
	MAT α , his3 Δ 200, leu2-3,112, ura3-52, lys2-801, vps1 Δ ::natNT2, SLA1-
MKY3346	EGFP::HIS3MX6
	MAT α , his3 Δ 200, leu2-3,112, ura3-52, lys2-801, vps1 Δ ::natNT2, SLA1-
MKY3347	EGFP::HIS3MX6 , ABP1-mCherry::kanMX4
MKY3559	MAT α , his3 Δ 200, leu2-3,112, ura3-52, lys2-801, Inp51-EGFP::HIS3MX6
MKY3560	MAT α , his3 Δ 200, leu2-3,112, ura3-52, lys2-801, Inp52-EGFP::HIS3MX6
MKY3561	MAT α , his3 Δ 200, leu2-3,112, ura3-52, lys2-801, inp51 Δ ::URA
	MAT α , his3 Δ 200, leu2-3,112, ura3-52, lys2-801, inp51 Δ ::URA, Sla1-
MKY3562	EGFP::HIS3MX6, Abp1-mCherry::KANMX4
MKY3586	MAT α his3 Δ 200, leu2-3,112, ura3-52, lys2-801 inp52 Δ ::hphNT1
MKY3587	MAT α his3 Δ 200, leu2-3,112, ura3-52, lys2-801 inp52 Δ ::hphNT1
	MAT α , his3 Δ 200, leu2-3,112, ura3-52, lys2-801, Rvs167-EGFP::HISMX6,
MKY3620	inp51 Δ ::URA
	MAT α , his3 Δ 200, leu2-3,112, ura3-52, lys2-801, Rvs167-EGFP::HISMX6,
MKY3621	inp51 Δ ::URA
	MAT α , his3 Δ 200, leu2-3,112, ura3-52, lys2-801, Rvs167-EGFP::HISMX6,
MKY3622	inp51 Δ ::URA
	MAT α , his3 Δ 200, leu2-3,112, ura3-52, lys2-801, Inp52-EGFP::HISMX6, Abp1-
MKY3623	mCherry::KANMX4
	MAT α , his3 Δ 200, leu2-3,112, ura3-52, lys2-801, Inp52-EGFP::HISMX6 Abp1-
MKY3624	mCherry::KANMX4
MKY3702	MAT α his3 Δ 200, leu2-3,112, ura3-52, lys2-801 RVS161::URA::RVS161
	MAT α , his3 Δ 200, leu2-3,112, ura3-52, lys2-801, RVS161::URA::RVS161,
MKY3703	RVS167::HPH::RVS167
	MAT α , his3 Δ 200, leu2-3,112, ura3-52, lys2-801, RVS161::URA::RVS161,
MKY3704	RVS167::HPH::RVS167
	MAT α his3 Δ 200, leu2-3,112, ura3-52, lys2-801 RVS167::HPH::RVS167, SLA1-
MKY3705	EGFP::HISMX6
	MAT α his3 Δ 200, leu2-3,112, ura3-52, lys2-801 RVS161::URA::RVS161
MKY3706	RVS167::HPH::RVS167 SLA1-EGFP::HISMX6 ABP1-mCherry::KANMX4
MKY3707	MAT α his3 Δ 200, leu2-3,112, ura3-52, lys2-801 RVS167::HPH::RVS167
	MAT α his3 Δ 200, leu2-3,112, ura3-52, lys2-801, Rvs167-
MKY3708	EGFP::his3MX6::hphNT1::Rvs167-EGFP::his3MX6
	MAT α his3 Δ 200, leu2-3,112, ura3-52, lys2-801 RVS167-EGFP::HPH::RVS167-
MKY3709	EGFP Abp1-mCherry

	MATa his3Δ200, leu2-3,112, ura3-52, lys2-801, RVS161::URA::RVS161, SLA1-
MKY3711	EGFP::HISMX, ABP1-mCherry::kanMX
	MATa, his3Δ200, leu2-3,112, ura3-52, lys2-801, Rvs167-
MKY3712	EGFP::his3MX6::hphNT1::Rvs167-EGFP::his3MX6, RVS161::URA::RVS161
MKY3713	MATα, his3Δ200, leu2-3,112, ura3-52, lys2-801, rvs167-ΔSH3::natN2
	MATα, his3Δ200, leu2-3,112, ura3-52, lys2-801, rvs167-ΔSH3-
	EGFP::his3MX6::hphNT1::rvs167-ΔSH3-EGFP::his3MX6, ABP1-
MKY3714	mCherry::kanMX
	MATα, his3Δ200, leu2-3,112, ura3-52, lys2-801, rvs167-ΔSH3-
	EGFP::his3MX6::hphNT1::rvs167-ΔSH3-EGFP::his3MX6, ABP1-
MKY3728	mCherry::kanMX, RVS161::URA::RVS161
	MATa his3Δ200, leu2-3,112, ura3-52, lys2-801, Rvs167-EGFP::HISMX6 Abp1-
MKY3803	mCherry::KANMX4
	MATα his3Δ200, leu2-3,112, ura3-52, lys2-801, inp52Δ::hphNT1, Abp1-
MKY3804	mCherry::kanMX4
	MATα his3Δ200, leu2-3,112, ura3-52, lys2-801, inp52Δ::hphNT1, Rvs167-
MKY3805	EGFP::HIS3MX6
	MATa his3Δ200, leu2-3,112, ura3-52, lys2-801, inp52Δ::hphNT1, Rvs167-
MKY3806	EGFP::HIS3MX6
	MATα, his3Δ200, leu2-3,112, ura3-52, lys2-801, rvs167-
	ΔSH3::natNT2::hphNT1::rvs167-ΔSH3::natNT2, SLA1-EGFP::HISMX, ABP1-
MKY3826	mCherry::kanMX
	MATα, his3Δ200, leu2-3,112, ura3-52, lys2-801, inp52Δ::hphNT1, SLA1-
MKY3827	EGFP::HISMX, ABP1-mCherry::kanMX
	MATa/ALPHA his3Δ200, leu2-3,112, ura3-52, lys2-801
	RVS161::URA::RVS161/RVS161::URA::RVS161, Rvs167-
	EGFP::his3MX6::hphNT1::Rvs167-EGFP::his3MX6/Rvs167-
	EGFP::his3MX6::hphNT1::Rvs167-EGFP::his3MX6, ABP1-
MKY3945	mCHerry::KANMX4/Abp1
	MATa/ALPHA, his3Δ200, leu2-3,112, ura3-52, lys2-801, Rvs167-
MKY3946	EGFP::HIS3MX6/Rvs167-EGFP::HIS3MX6, ABP1-mCHerry::KANMX4/Abp1
	MATa/α, his3-delta200, leu2-3,112, ura3-52, RVS167-
	EGFP::HIS3MX6/rvs167delta::cgLEU2, rvs161delta::cgLEU2/RVS161, ABP1-
MKY3947	RFP::HIS3MX6/ABP1
MKY3948	MATa, his3Δ200, leu2-3,112, ura3-52, lys2-801, Inp53-EGFP::HIS3MX6

5.1.2 Plasmids

Plasmid cassettes used for endogenous tagging and gene deletions/ duplication.

Name	Purpose
pFA6a-EGFP-HIS4MX	EGFP tag
pFA6a-mCherry-KanMX4	mCherry tag
pFA6a-natNT2	deletion
pks133	deletion, duplication
pFA6a-KiUra	deletion

5.1.3 Buffers

PEG buffer

Lithium acetate	100 mM
Tris-HCl pH 8	10 mM
EDTA pH 8	1 mM
Polyethylene glycol	4 % w/v

SORB buffer

Lithium acetate	100 mM
Tris-HCl pH 8	10 mM
EDTA pH 8	1 mM
Sorbitol	1 M

S buffer

K2HPO4 pH 7.2	10 mM
EDTA	10 mM
β-mercaptoethanol	50 mM
Zymolyase	50 µg/mL

Lysis Buffer

Sodium dodecyl sulphate (SDS)	2.5 % w/v
Tris-HCl pH 7.5	25 mM
EDTA	25 mM

5.1.4 Media

Media was kindly prepared by the EMBL and University of Geneva media kitchens, and by Anne-Sophie Riviera. Plates containing media were made by adding 2% w/v bacto agar.

Yeast extract Peptone Dextrose (YPD)

BactoYeast Extract	1 % w/v
Bacto Peptone	2 % w/v
Glucose	2 % w/v

Synthetic Complete (SC)

DifcoTM Yeast nitrogen base w/o amino acids	0.67 % w/v
Glucose	2 % w/v
Amino acid stock (SC)	10 % v/v

Amino acid stock (SC) –dissolved in 100 mL

H2O

Adenine	0.5 g
Leucine	10 g
Alanine, Arginine, Asparagine, Aspartic acid, Cysteine, Glutamine, Glutamic acid, Glycine, Histidine, Inositol, Isoleucine, Lysine, Methionine, para-Aminobenzoic acid, Phenylalanine, Proline, Serine, Threonine, Tryptophan, Tyrosine, Uracil, Valine. For auxotrophic selection, one amino acid is left out	
	2 g each

Sporulation plates

Potassium acetate	1 % w/v
Bacto Agar	2 % w/v
Amino acid stock (sporulation plate)	0.25 % v/v

Amino acid stock (sporulation plate)

Uracil, Histidine, Methionine	0.2 g
Leucine, Lysine	0.3 g

Antibiotic selection plates

Hygromycin B (Hph) (InvivoGen)	300 mg/L
Geneticin disulphate salt (G418) (Sigma)	200 mg/L
Nourseothricin (clonNAT) (Werner BioAgents)	100 mg/L

5.1.5 Imaging

Live-cell tracking

Microscope	IX81	Olympus
Objective	PlanApo 100x/1.45 TIRFM	Olympus
Camera (molecule number quantification)	Orca -ER	Hamamatsu
Fluorescent lamp (molecule number quantification)	X-CITE 120 PC	EXFO
Laser source for GFP excitation	Sapphire 488-100	Coherent
Laser source for RFP excitation	Compass 315M (561 nm)	Coherent
Camera	ImagEM EMCCD	Hamamatsu
Microscope (TIRF)	IX83	Olympus
Camera (TIRF)	Image mX2 EMCCD	Hamamatsu
Objective (TIRF)		
Laser source (TIRF)	VS-LMS	Visitron

Electron microscopy

Microscope	Tecnai F30 300kV FEG	FEI
Camera	4k Eagle	FEI

5.2 Methods

5.2.1 Fluorescent tagging yeast with PCR cassette insertion

Tagging or deletion of endogenous genes was done by homologous integration of the product of a Polymerase Chain Reaction using appropriate primers and a plasmid containing a selection cassette and fluorescent tag, or only selection cassette for gene deletions. Primers were designed according to Janke et al, 2004. PCRs used the Velocity Polymerase for fluorescent tagging, and Q5 for gene deletions using the NAT cassette. All fluorescently tagged genes have a C-terminus tag and are expressed endogenously. Gene deletions and fluorescent tags are checked by PCR. Vps1del and gene duplications were confirmed by sequencing.

5.2.2 Live-cell imaging

Sample preparation for live imaging

40 µL Concanavalin A (ConA) was incubated on a coverslip for 10 minutes. 40 µL Yeast cells incubated overnight at 25C in imaging medium SC-TRP was added to the coverslip after removing the ConA, and incubated for another 10 minutes. Cells were then removed, adhered cells were washed 3x in SC-TRP, and 40 µL SC-TRP was finally added to the coverslip to prevent cells from drying.

Sample preparation for live imaging in LatA and Sorbitol treated cells

Cells went through the same procedure as above till the last washing step. Instead of SC-TRP, 100x diluted LatA, or Sorbitol at a final concentration of 0.2M in SC-TRP was added to the adhered cells. For LatA experiments, cells were incubated in LatA for 10 minutes before imaging. For sorbitol treatments, cells were imaged within 5 minutes of adding sorbitol.

Epifluorescent imaging for centroid tracking

Live-cell imaging was performed as in Picco et al. All images were obtained at room temperature using an Olympus IX81 microscope equipped with a 100×/NA 1.45 PlanApo objective , with an additional 1.6x magnification lens and an EMCCD camera. The GFP channel was imaged using a 470/22 nm band-pass excitation filter and a 520/35 nm band-pass emission filter. mCherry epifluorescence imaging was carried out using a 556/20 nm band-pass excitation filter and a 624/40 band-pass emission

filter. GFP was excited using a 488 nm solid state laser and mCherry was excited using a 561 nm solid state laser. Hardware was controlled using Metamorph software. For single-channel images, 80-120ms was used as exposure time. All dual-channel images were acquired using 250ms exposure time. Simultaneous dual-color images were obtained using a dichroic mirror, with TetraSpeck beads used to correct for chromatic abberation.

Epifluorescent imaging for molecule number quantification

Images were acquired as in Picco et al. Z-stacks of cells containing the GFP-tagged protein of interest, incubated along with cells containing Nuf2-GFP, were acquired using 400ms exposure using a mercury vapour lamp, on a CCD camera. Z stacks were spaced at 200nm.

TIRF imaging

TIRF microscopy was performed under similar conditions on an Olympus IX83 microscope. GFP was excited using a 488 nm solid state laser and mCherry was excited using a 561 nm solid state laser. Lasers, and shutters were controlled by Visitron Systems VS-Laser Control. VisiView software controlled the image acquisition and hardware-software feedback. Images were processed using ImageJ, quantification was done on R.

5.2.2.1 Live-cell Image analysis

Images were processed for background noise using a rolling ball radius of 90 pixels. Particle detection, and tracking was performed for a particle size of 6 pixels, using scripts that combine background subtraction with Particle Tracker and Detector, that can be found on ImageJ (<http://imagej.nih.gov>). Further analysis for centroid averaging, alignments between dual-color images and single channel images, for alignment to the reference Abp1 were done using scripts written in Matlab (Mathworks) and R (www.r-project.org), written originally by Andrea Picco, and modified by me. Details of analysis can be found at Picco et al. All movement and intensity plots from centroid tracking show the average centroid with 95% confidence interval. All molecule number quantifications report either the median or maximum number of molecules with standard error of mean. Maximum number is preferred over median in cases when the rate of change of fluorescent intensity of two populations being compared are not similar, and the lifetime of the protein populations being compared are not similar. The median in this case underreports the differences in protein accumulation.

5.2.2.2 Cytoplasmic background quantification for BAR versus WT Rvs167-GFP

On a maximum intensity projection of time-lapse images, the average pixel intensity within a circle of set radius in the cytoplasm was measured. This circle is manually arranged so that cortical patches were excluded, and mean intensity was acquired for about 10 cells of each cell type. A fixed area outside the cells was drawn, and mean intensity was calculated to establish "background intensity". This background intensity was then subtracted from the mean intensity to obtain a rough measure of cytoplasmic intensity. The same was done for endocytic spots. For WT strain, cytoplasmic signal after subtracting background is measured as 1951.611 +/- 299.56 (arbitary units, average +/- SEM), with spot intensity 5486 +/- 1304.6 (arbitary units, average +/- SEM). For BAR strain, cytoplasmic signal is 2058 +/- 322 (arbitary units, average +/- SEM), spots are 4477 +/- 1144.7 (arbitary units, average +/- SEM). The ratio of spot intensity for WT to BAR strain is 1.22, so the WT spots are 1.2x brighter than the BAR spots measured in this way. Cytoplasmic background of BAR is comparable to that of the WT: the ratio of WT to BAR cytoplasmic signal obtained in this way is 0.94. Although this is not a stringent quantification of cytoplasmic intensity, with some caveats: the cells were not incubated in the same field of view, cellular autofluorescence is assumed to be equal for the two cell types, I take this measurement to indicate that the cytoplasmic content of BAR and WT Rvs167-GFP is not significantly different.

5.2.2.3 CLEM

Samples were prepared for CLEM as described in Wanda et al. Briefly, cells expressing Rvs167-GFP and Abp1-mCherry, and BAR-GFP and Abp1-mCherry cells were grown overnight in YPD, at 24C. They were then diluted to an OD600 of 0.2, and grown to OD600 between 0.8 and 1.2. These cells were then concentrated to a filter paper using a vacuum pump, and high-pressure frozen. Samples were freeze substituted in Lowycryl HM20 using the Kukulski freeze substitution protocol using an automated robot. Samples in resin were sliced to 300nm sections using a diamond knife, and loaded to carbon-coated copper grids. TetraSpec beads were incubated on the slices and these slices were imaged using epifluorescence microscopy in GFP and RFP channels for GFP and m-Cherry, and Cyan channel for separating the signal from the Tetraspec beads, that would later be used as fiducials to correlate these fluorescent images with electron

tomograms. Gold fiducials were incubated on the grids, and lead citrate was added to stain the membrane. Low magnification tilts were acquired at 3 degree increments. High magnification tilts were performed at 1 degree increments from -60 to 60 degrees. Tomograms were reconstructed using IMOD. Invagination lengths were measured at the longest axis of the invagination, using IMOD.